

Geostatistical and Spatial Statistical Modelling of Precipitation Variations in Iran

Majid Javari*

College of Social Sciences, Payame Noor University, Iran PO BOX 19395-3697, Tehran, Iran

Abstract

This study examines the geostatistics and spatial relationships between annual, seasonal and monthly rainfall in Iran for the period 1975-2014. Precipitation variation models were compared in Iran deriving from six geostatistical, four regression and five spatial models, using monthly data. A geostatistical and spatial statistical analysis consisting of two measurement sub-models was created based on monthly accumulated precipitation; the data was the monthly and seasonal amounts for the period 1975 - 2014, and were estimated from 140 stations. The results of the new geostatistical-spatial statistical analysis model showed that average monthly precipitation series in Iran were revealed to follow Gaussian distribution given their histogram plots and closeness of their mean and median values. On average, monthly precipitation ranged from 3.22 mm in April to 47.157 mm in December in Iran. The suitable interpolation of monthly precipitation indicates that the accuracy of spring precipitation interpolation (RMSE=0.558) can be applied by IDW (Cross-validation). The kriging interpolation of monthly precipitation indicates that the accuracy of autumn precipitation interpolation (RMSE=0.0822) can be applied by probability kriging of autumn precipitation. The empirical Bayesian kriging interpolation of monthly precipitation indicates that the accuracy of autumn precipitation interpolation (RMSE=0.357) can be applied by empirical Bayesian kriging of autumn precipitation. The temporal-spatial distribution of the precipitation station locations has been studied using the ANN tool of the spatial statistics toolbox of ArcGIS 10.3. Based on the calculated Moran's Index, approximately all months' precipitation (with the exception of February) has the monthly spatial distribution of the clustered type. The High/Low Clustering of stations' monthly precipitation has been studied using the HLC tool. Based on the calculated g-index, approximately all months' precipitation (except for February and March) has the monthly spatial distribution of the high-clusters type.

Keywords: Geostatistical modeling; Geostatistical-spatial model, Geostatistical-spatial variations; Precipitation variations; Precipitation

Introduction

Precipitation is one of the input variables for temporal-spatial variations system evaluation and characterization patterns, as well as hydro-climatic and environmental models [1,2]. These models use precipitation to drive processes such as drought, erosion, and hydro-morphology processes [3-5]. Hence, water source management and research need these precipitation variations as a basis for understanding many processes, as it is the main factor affecting precipitation patterns, in the sense that its action is felt over areas of the earth's surface process [6-8]. Monthly precipitation is an important element city properties used in determining city development for agriculture and commercial productions and tourism industry [9-11]. Moreover, monthly precipitation is a factor related to hydrological patterns, as it is connected with the variations of the rainfall period and water balance elements [12,13].

Therefore, geostatistical-spatial modelling of climatic elements, such as monthly precipitation, is of interest for climatologists and hydrologist [1,14,15]. Different interpolation methods have been used to model the geostatistical spatial patterns of monthly precipitation. The most widely used interpolation techniques are deterministic and geostatistical methods, deterministic interpolation techniques, global and local models, Inverse Distance Weighting (IDW) and kriging interpolation, Voronoi mapping, least squares analysis or more recently, geostatistical-spatial statistical methods [4,16-19]. Several researchers have compared different methods (splines, inverse distance weighting, Kriging and Cokriging and types of kriging) for monthly precipitation in various parts of world [20-23].

These methods can be used to produce the following surfaces: maps of kriging predicted values, maps of kriging standard errors associated with predicted values, maps of probability, indicating whether or not a predefined critical level was exceeded and maps of quantile for a predetermined probability level. Geostatistical (kriging) models

comprise several components: examining the precipitation variations (distribution, trends, directional components, outliers), calculating the empirical semivariogram or covariance precipitation, fitting a model to the empirical values, generating the matrices of kriging equations, and solving them to obtain a predicted precipitation and the error associated with it for station location in the output surface [11,24-26].

Geostatistical-spatial methods such as kriging and Average Nearest Neighbor were generally developed for spatial statistical analysis of precipitation, but have since been applied to a number of other techniques, including spatial interpolation precipitation. Kriging and cokriging consist of three steps: an examination of precipitation values covariance, fitting theoretical models to precipitation spatial relationships and using these models to calculate the weights for neighboring station points and calculating the interpolated precipitation values [7,17,25,27,28]. However, recent advances in precipitation variations modelling of climatic analysis now enable a consistent, geostatistical-spatial evaluation of expert knowledge as the basis for modeling; specifically through the geostatistical-spatial statistical models [29-32].

This study aimed to compare different geostatistical-spatial approaches and kriging and cokriging models and Average Nearest Neighbor (ANN), High/Low Clustering (HLC), spatial autocorrelation (SAU), Multi-Distance Spatial Cluster Analysis (MDSCA) and Incremental Spatial Autocorrelation (ISAU) and the ordinary least

*Corresponding author: College of Social Sciences, Payame Noor University, Iran, PO BOX 19395-3697, Tehran, Iran, Tel: 09133285930; E-mail: ananthm@intecc.com

Received August 09, 2015; Accepted May 08, 2016; Published May 10, 2016

Citation: Javari M (2016) Geostatistical and Spatial Statistical Modelling of Precipitation Variations in Iran. J Civil Environ Eng 6: 230. doi:10.4172/2165-784X.1000230

Copyright: © 2016 Javari M, et al. This is an open-access article distributed under the terms of the Creative Commons Attribution License, which permits unrestricted use, distribution, and reproduction in any medium, provided the original author and source are credited.

squares (OLS) residuals to spatially predict monthly precipitation in 1975-2014 in Iran. We also investigated the precipitation trend spatial variations. Geostatistical-spatial model can be employed as a versatile GIS technique to provide a suitable framework for the spatial variations analysis of precipitation patterns and precipitation variations. The rest of the paper is organized as follows: in Sect. 4, we briefly introduce the geostatistical model and the spatial statistical methods to provide a description of our proposed spatial effects framework of precipitation that is explained in the next section. Sect. 5 presents the new modeling of precipitation variations in detail. The experimental results and conclusions are presented in Sects. 6 and 7 respectively.

Background

This paper employs the geostatistical-spatial statistical analysis methods for investigating the variations in precipitation patterns. The next subsections provide a brief introduction to these two algorithms to make this paper more reader-friendly and self-contained. Algorithm 1 represents a geostatistics algorithm which consists of three stages. The geostatistics algorithm includes the following three steps in Algorithm 1 [24,33-40]:

<p>Algorithm 1 - The geostatistics method:</p> <p>Step 1: Geostatistics as a means to study precipitation variations:</p> <p>1-Exploratory of precipitation spatial patterns:</p> <p>a.Histogram Plot</p> <p>Normal QQ Plot: $f(p, h) = Prob[Z(s) \leq z_p, Z(s+h) \leq z_p]$</p> <p>Trend analysis: $\mu_{(s)} = \beta_0 + \beta_1x + \beta_2y + \beta_3x^2 + \beta_4y^2 + \beta_5xy$, $Z(s) = \mu(s) + \varepsilon(s)$</p> <p>Voronoi map</p> <p>Semivariogram / covariance cloud: $\gamma(h) = \frac{1}{2n(h)} \sum_{i=1}^{n(h)} [Z(x_i) - Z(x_i+h)]^2$,</p> <p>General QQ plot.</p> <p>Crosscovariance. cloud: $\gamma_{uv}(h) = \frac{1}{2n(h)} \sum_{i=1}^{n(h)} [Z_u(x_i) - Z_u(x_i+h)][Z_v(x_i) - Z_v(x_i+h)]$</p> <p>2-Examining local variation of precipitation.</p> <p>Voronoi mapping:</p> <p>1-Simple</p> <p>2-Mean</p> <p>3-Mode</p> <p>4-Cluster</p> <p>5-Entropy</p> <p>6-Median</p> <p>7-Standard deviation</p> <p>8-Interquartile range</p> <p>Prediction performances were assessed by cross-validation: $RMSE = \sqrt{\sum (Z_i - \hat{Z}_i)^2} / n$</p> <p>3-Identify global trends in monthly precipitation:</p> <p>1- Linear trend.</p> <p>4-Exploration of spatial autocorrelation and directional influences in Iran Precipitation:</p> <p>1-semivariogram</p> <p>2- autocorrelation</p> <p>3- Spatial statistical analysis</p> <p>5-Explanation of Iran monthly precipitation:</p> <p>Inverse distance weighted (IDW) interpolation: $\hat{Z}(u_s) = \sum_{i=1}^n z(u_i)w_i / \sum_{i=1}^n w_i$</p> <p>Kriging and Cokriging interpolation :</p> <p>Ordinary : $Z(s) = \mu + \varepsilon(s)$</p> <p>Simple : $Z(s) = \mu + \varepsilon(s)$</p> <p>Universal : $Z(s) = \mu(s) + \varepsilon(s)$</p> <p>Indicator : $I(s) = \mu + \varepsilon(s)$</p> <p>Probability : $I(s) = I[Z(s) > C_i] = \mu_1 + \varepsilon_1(s)$, $Z(s) = \mu_2 + \varepsilon_2(s)$,</p> <p>Disjunctive: $\hat{g}(Z(s_i)) = \sum_{i=1}^n f_i(Z(s_i))$, $fZ(s) = \mu_1 + \varepsilon(s)$,</p> <p>Cokriging : $Z_1(s) = \mu_1 + \varepsilon_1(s)$, $Z_2(s) = \mu_2 + \varepsilon_2(s)$,</p> <p>Empirical Bayesian</p> <p>6- Semivariogram/Covariance modeling:</p> <p>Semi-variogram: $\gamma(s_i, s_j) = 1/2 \text{var}(Z(s_i) - Z(s_j))$,</p> <p>Semi-variogram: $C(s_i, s_j) = \text{cov}(Z(s_i), Z(s_j))$</p> <p>Semivariogram/Covariance Relationship : $\gamma(s_i, s_j) = sill - C(s_i, s_j)$, $Z(s) = \mu(s) + \varepsilon(s) + \delta(s)$, $average[(z(s_i) - \bar{z})(z(s_j) - \bar{z})]$</p> <p>Gaussian: $\gamma(h, \theta) = \theta_s \left[1 - \exp\left(-3 \left(\frac{ h }{\theta}\right)^2\right) \right]$, where $\theta_s \geq 0$ is the partial sill parameter and $\theta_r \geq 0$ is the range parameter.</p> <p>1-Normal QQ plot and general QQ plot.</p> <p>The Cross-covariance cloud plotting: $C_{km}(s_i, s_j) = \text{cov}(Z_k(s_i), Z_m(s_j))$, $average[(z_1(s_i) - \bar{z}_1)(z_2(s_j) - \bar{z}_2)]$,</p> <p>Step 2: Comparison of methods results.</p> <p>Step 3: Mapping of selective methods.</p>

In this study, the spatial variations of the monthly, seasonal and annual rainfall and temperature were determined using the spatial statistics analysis (SSA) technique. Spatial data analysis is a statistical method of certain climate manifested in spatial. The tools available for exploratory of precipitation spatial patterns in the geostatistical analysis include: histogram, normal QQ plot, trend analysis, Voronoi diagram, semivariogram / covariance cloud, general QQ plot, and cross-covariance cloud. Special techniques and methods are developed for classification of precipitation which has topological, climatic and hydro-climatic properties. The basic SSA algorithm, as suggested, includes the following three steps in Algorithm 2 [19,36,41-43].

Algorithm 2 - The spatial statistics analysis:

Step 1: Analyzing patterns of precipitation :

Average nearest Neighbor : $ANN = \bar{D}_O / \bar{D}_E$, $\bar{D}_O = \sum_{i=1}^n d_i / n$, $\bar{D}_E = 0.5 / \sqrt{n/A}$, $Z = \frac{\bar{D}_O - \bar{D}_E}{SE}$, $SE = 0.26136 / \sqrt{n^2/A}$

High/Low Clustering (Getis-Ord General G): $G = \sum_{i=1}^n \sum_{j=1}^n w_{i,j} x_i x_j / \sum_{i=1}^n \sum_{j=1}^n x_i x_j$,

Incremental Spatial Autocorrelation : $I = \frac{n}{S_o} \sum_{i=1}^n \sum_{j=1}^n w_{i,j} z_i z_j / \sum_{i=1}^n z_i^2$, $S_o = \sum_{i=1}^n \sum_{j=1}^n w_{i,j}$, $Z_1 = \frac{1 - E[I]}{\sqrt{V[I]}}$

Multi-Distance Spatial Cluster Analysis (Ripley's K Function): $L(d) = \sqrt{A \sum_{i=1}^n \sum_{j=1, j \neq i}^n k_{i,j} / \pi n(n-1)}$

Spatial Autocorrelation (Global Moran's I): $I = \frac{n}{S_o} \sum_{i=1}^n \sum_{j=1}^n w_{i,j} z_i z_j / \sum_{i=1}^n z_i^2$

Step 2: Mapping clusters:

Cluster and Outlier Analysis (Anselin Local Moran's I): $I_i = \frac{x_i - \bar{X}}{S_i^2} \sum_{j=1, j \neq i}^n w_{i,j} (x_j - \bar{X})$, $S_i^2 = \frac{\sum_{j=1, j \neq i}^n (x_j - \bar{X})^2}{n-1} - \bar{X}^2$

Hot Spot Analysis (Getis-Ord Gi):

$$G_i^* = \sum_{j=1}^n w_{i,j} x_j - \bar{X} \sum_{j=1}^n w_{i,j} / S \sqrt{\frac{n \sum_{j=1}^n w_{i,j}^2 - \left(\sum_{j=1}^n w_{i,j} \right)^2}{n-1}}$$

$$\bar{X} = \sum_{j=1}^n x_j / n, S = \sqrt{\sum_{j=1}^n x_j / n - (\bar{X})^2}$$

-Optimized hot spot analysis.

Step 3: Modeling spatial relationships :

Exploratory regression : $\mu(s) = \beta_0 + \beta_1 x + \beta_2 y + \beta_3 x^2 + \beta_4 y^2 + \beta_5 xy$, $\hat{Z}(s_o) = \sum_{r,s \in N} a_{rs} x^r, y^s = a^T | .s_o$,

Geographically weighted regression: $GWR = \beta_0 + \beta_1 + \beta_2 + \dots + \beta_n + \epsilon_n$

Ordinary least squares (OLS): $y = \beta_0 + \beta_1 x + \beta_2 x_2 + \dots + \beta_n x_n + \epsilon$

Step 4: Comparison of methods results

Step 5: Mapping of selective methods: $\hat{Z}(s_o) = \sum_{i=1}^n w_i \times z(s), w_i \begin{cases} 1/n_k \text{ for } x_i \in k \\ 0, \text{ otherwise} \end{cases}$

Step 6: Extraction of results and final mapping of results

Materials and Methods

Materials

Iran, situated in the southwest of Asia, ranges from 25° 3' to 39° 47' N and from 44°5' to 63°18' E. The case study deals with the identification of geostatistics and spatial statistics effect on precipitation to better forecast the precipitation variations in Iran. Precipitation variations can be defined from various aspects, such as effectiveness of precipitation formation factors or even climatic events such as drought. With regard to precipitation changes in Iran, we chose rainfall indices, namely. The chosen indices were obtained from meteorological organization and included the monthly, seasonal and annual information of 140 stations in Iran for the period 1975-2014 (Figure 1). All the observed precipitation data have been subject to strict quality control obtained [44]. The study focused on monthly, seasonal and annual variations. For this purpose, a harmonic analysis was applied to all data, and data was studied with respect to the time defaults, linearity, normality, missing data, outliers etc. at different phases of the research.

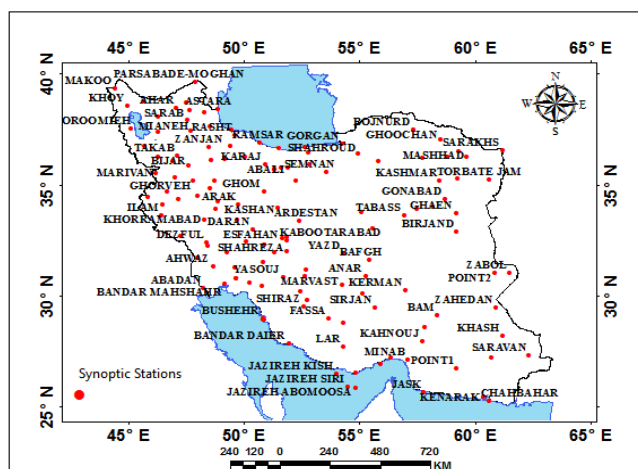


Figure 1: Location of synoptic stations.

Methods

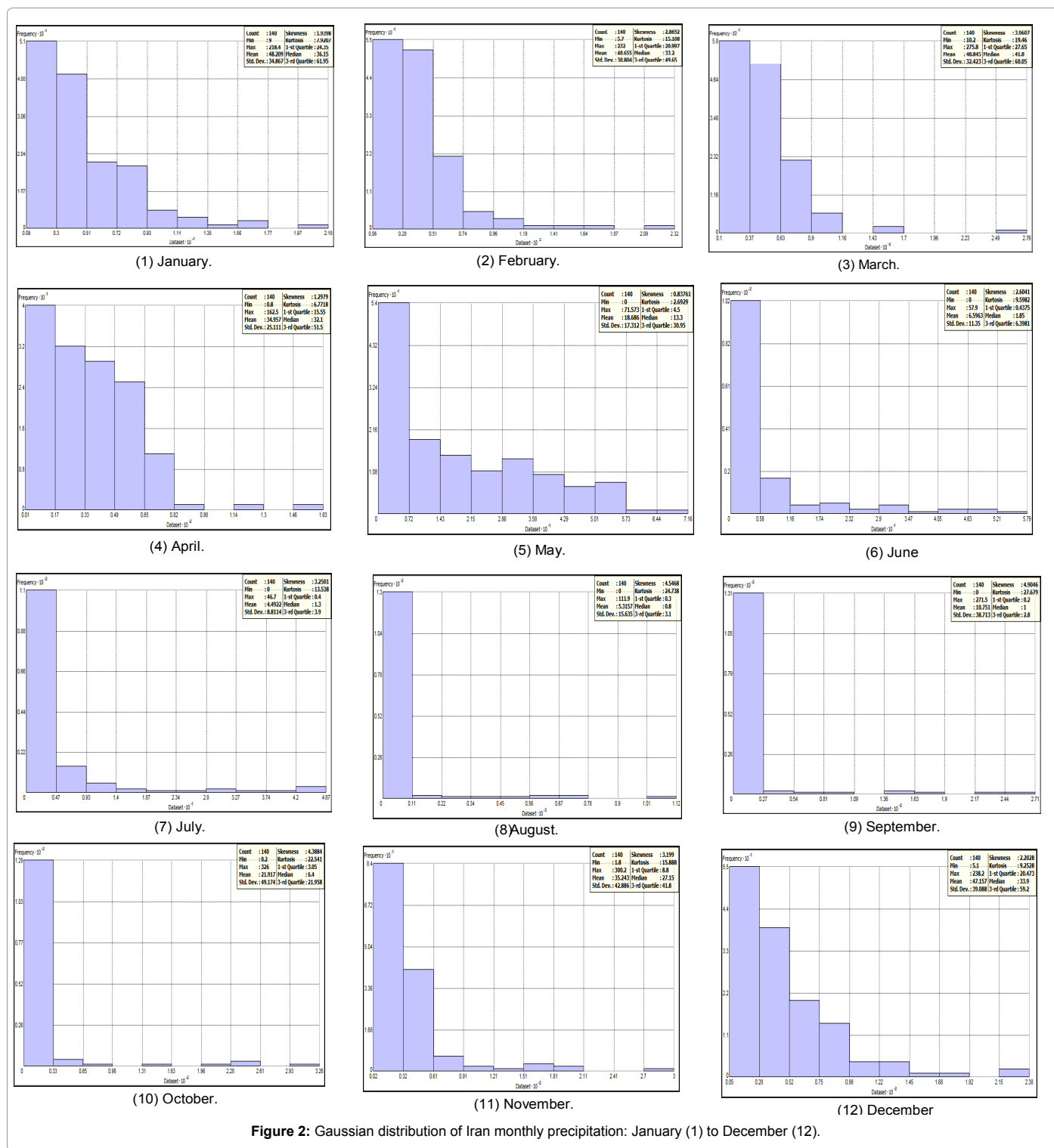
Prediction of precipitation patterns changes are based on geostatistical and spatial statistics analyses with the incorporation of monthly, seasonal and annually variations of predictor variables on response variables. Geostatistics and spatial model is a multivariate statistical technique that uses factor analysis, geostatistics analysis and spatial analysis to evaluate the relationship between precipitation variables. Application of this model in climatology leads to this question of how the spatial and geostatistics relationships among variables and the climatic factors are studied. Geostatistics analysis can be used to answer this question. Geostatistics is a subset of statistics specialized in analysis and interpretation of geographically referenced data [36,45,46].

Geostatistics is a class of statistics used to analyze and predict the precipitation associated with spatial or spatiotemporal precipitation. It incorporates the spatial-temporal coordinates of the precipitation within the analyses. Geostatistics is a collection of quantitative techniques for the measurement of spatial attributes using primarily two tools: probabilistic models, which are used for spatial data in a manner similar to the way in which time series analysis characterizes temporal data, or pattern recognition techniques [47,48].

Geostatistics is a type of statistics used to analyze and predict the precipitation associated with spatial or spatial-temporal rainfall variations [49,50]. The first stage suggests methods based on their ability to generate predictions or predictions and associated errors. The second stage suggests methods based on their ability to model spatial autocorrelation require defining precipitation values and interactively fitting a model to the precipitation. Different methods generate different types of output (predication, predication errors, kriging and simulation of precipitation). Interpolation methods vary in their levels of complexity, which can be measured by the number of assumptions that must be met for the model to be valid [45,51]. Geostatistics analysis required a range of neighbor points to take rainfall value for final analysis, maximum and minimum 20 neighbor values are 4 applied respectively [52,53].

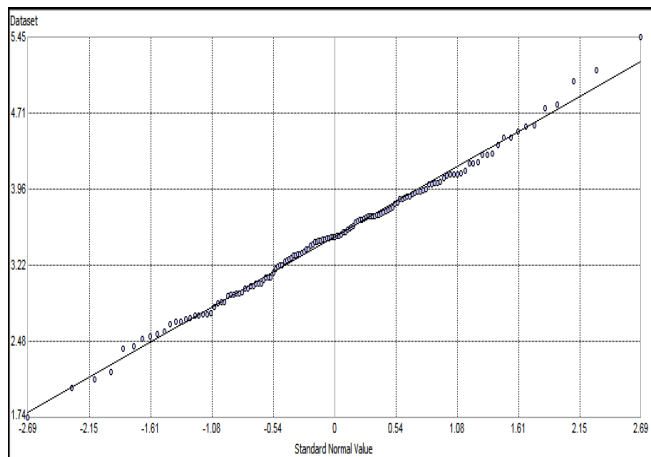
Exploratory of precipitation spatial patterns: The tools available for exploratory of precipitation spatial patterns in the geostatistical analysis include: histogram, normal QQ plot, trend analysis, Voronoi diagram, semivariogram / covariance cloud, general QQ plot, and cross-covariance cloud. The histogram tool provides a description of precipitation frequency distribution. Measures of any station location (mean, median and quartiles) provide with an idea of where the center and other parts of the stations distribution lie. The mean provides a measure of the distribution center. The median provides another measure of the stations distribution center. The first and third quartiles correspond to the cumulative proportion of 0.25 and 0.75, respectively. Measures of stations spread around the mean value is another characteristic of the displayed frequency distribution [54,55]. Measures of shape by coefficient of skewness are a measure of the symmetry of a distribution. For symmetric distributions, the coefficient of skewness is zero [36,56]. If a distribution has a long right tail of large values, it is positively skewed, and if it has a long left tail of small values, it is negatively skewed. The mean value was higher than the median value and the bias coefficient was greater than zero, indicating that the frequency distribution was skewed to the right and did not follow the normal distribution. The mean is larger than the median for positively skewed distributions and vice versa for negatively skewed distributions [36,57,58]. The kurtosis of a normal distribution is equal to three. The probability distribution function is to a long-term precipitation series, which is then transformed into a normal distribution [38,54,59]. To test the precipitation patterns variations, we performed a confirmatory and exploratory spatial analysis, which identifies the most likely temporal-spatial links among correlated rainfall variables. We studied the histogram, normal QQ plot, trend analysis, Voronoi diagram, semivariogram / covariance cloud, general QQ plot, and cross covariance cloud between monthly, seasonal and annual precipitation. Spatial and geostatistical patterns variations of Iran precipitation is highly related to the temporal-spatial link between monthly, seasonal and annually precipitation. Nevertheless, geostatistical-spatial effects could influence precipitation, which in turn affects amount, with no direct link between precipitation patterns. Moreover, geostatistical-spatial patterns differences could also directly influence precipitation. We studied histogram and normal QQ plot patterns, possible geostatistical-spatial effect, linkage models for each measure of precipitation variations at each stage (Figures 2 and 3).

Examining local variations of precipitation: The Voronoi diagram displayed areas of high standard deviation relative to neighboring values. The map showed that the greatest differences in precipitation are concentrated in Western half of the map. We studied the seasonal and annual

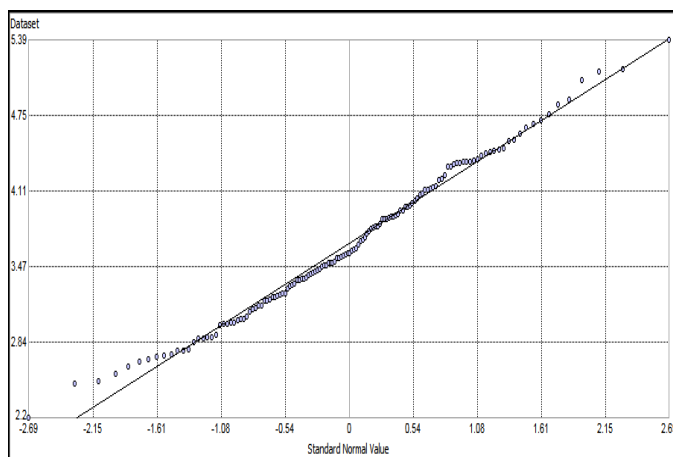


Voronoi diagrams to simple, mean, mode, cluster, entropy, median, standard deviation and interquartile range methods. Moreover, Voronoi diagrams differences could also directly influence precipitation. We used Voronoi diagrams to examine local variations of seasonal and annual precipitation series for every station. Voronoi diagrams are composed of a series of polygons formed around the location of a sample point (Figures 4 and 5).

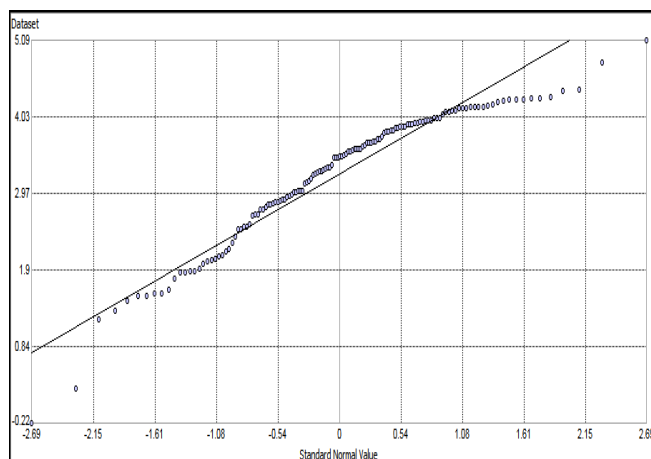
Identifying global trends in monthly precipitation: Voronoi diagram displayed areas of high standard deviation relative to neighboring values and greatest differences in precipitation are concentrated in Western half of the map. We used Voronoi diagrams to examine local variation of monthly, seasonal and annual precipitation series for every station. Voronoi diagrams are generated using the stations based on distance to



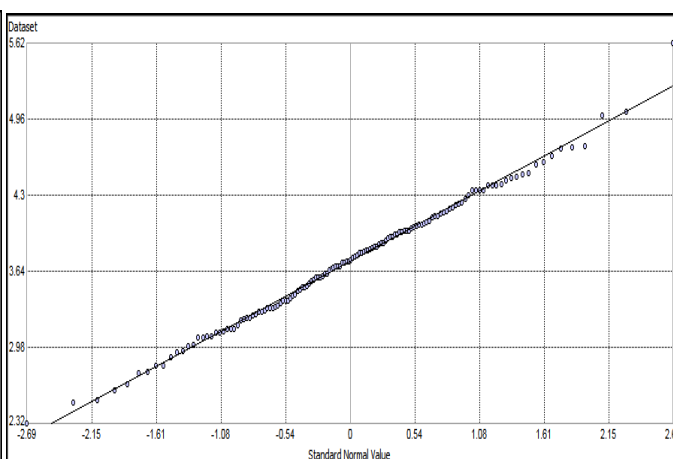
(2) February.



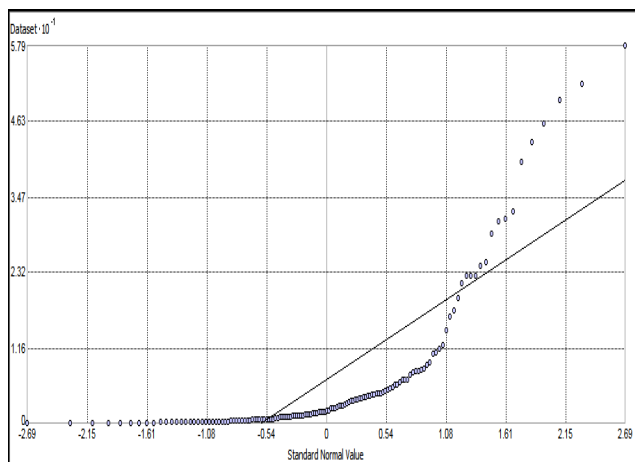
(1) January.



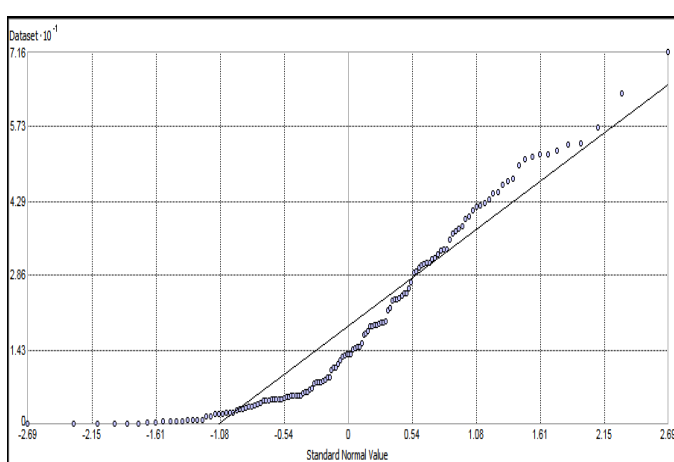
(4) April.



(3) March.



(6) June.



(5) May.

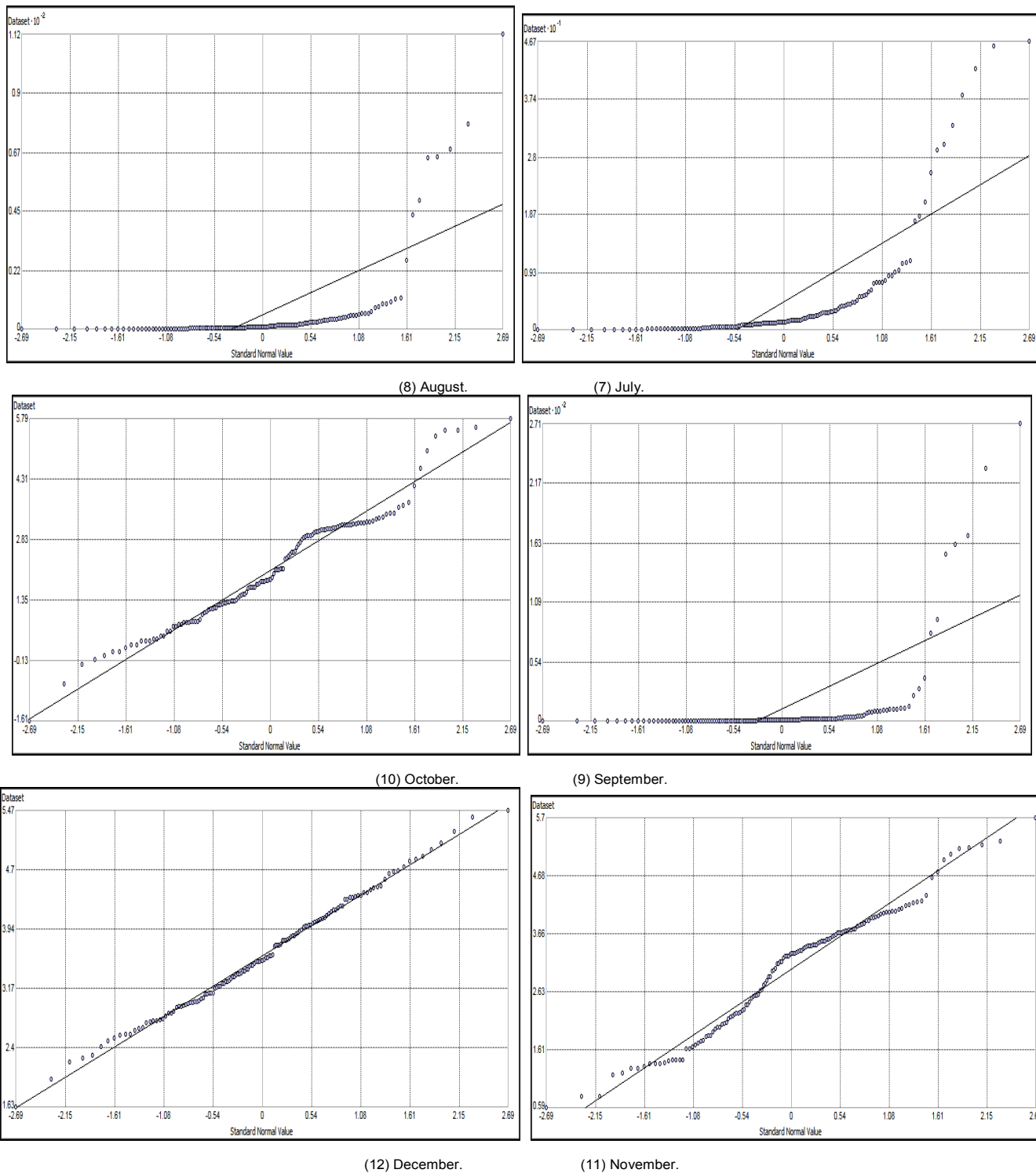
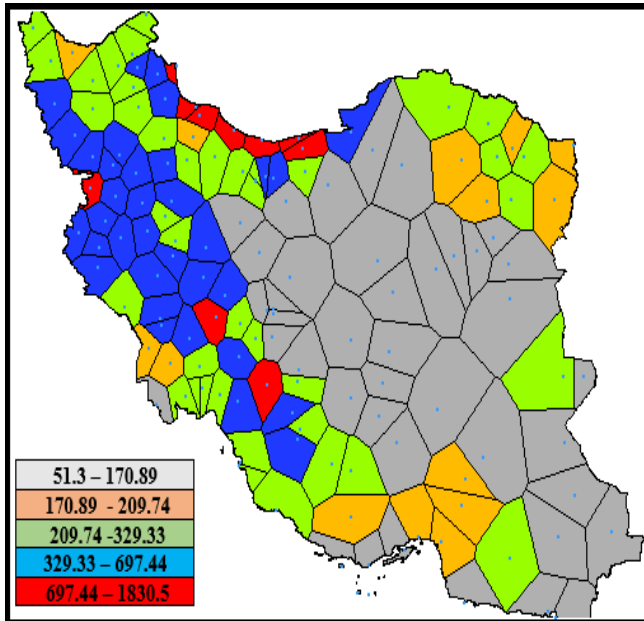
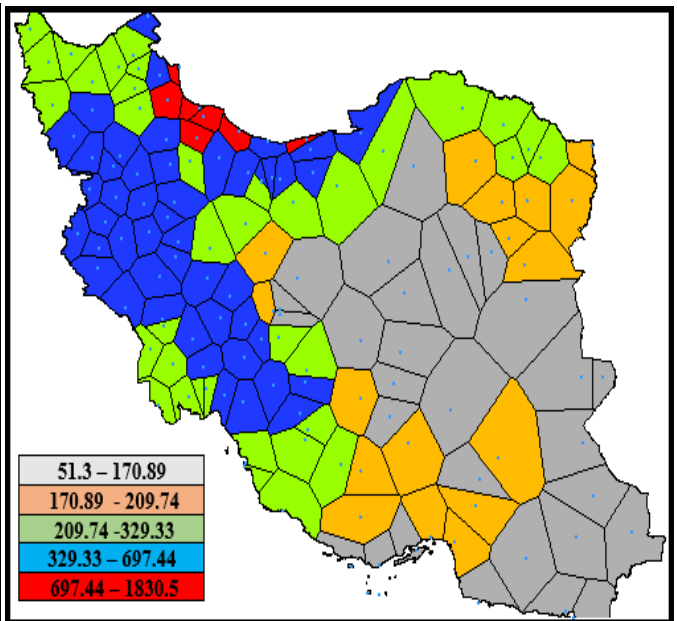


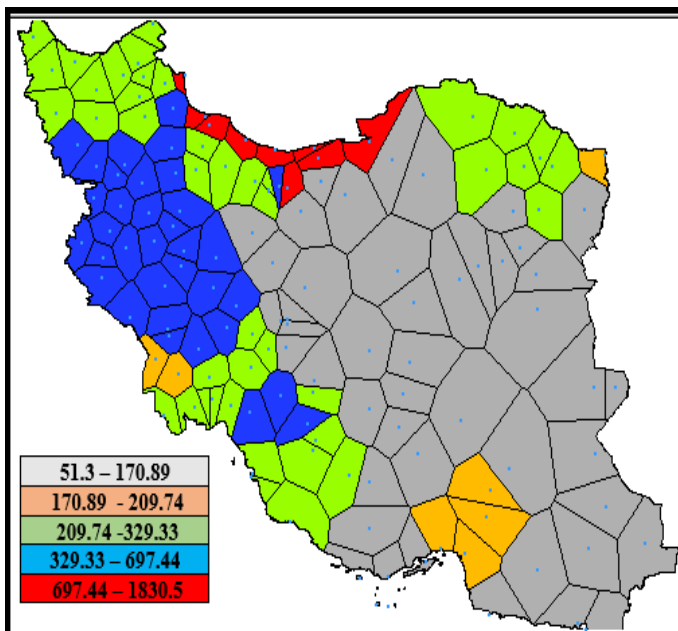
Figure 3: Statistical normality of monthly precipitation data of January (1) to December (12).



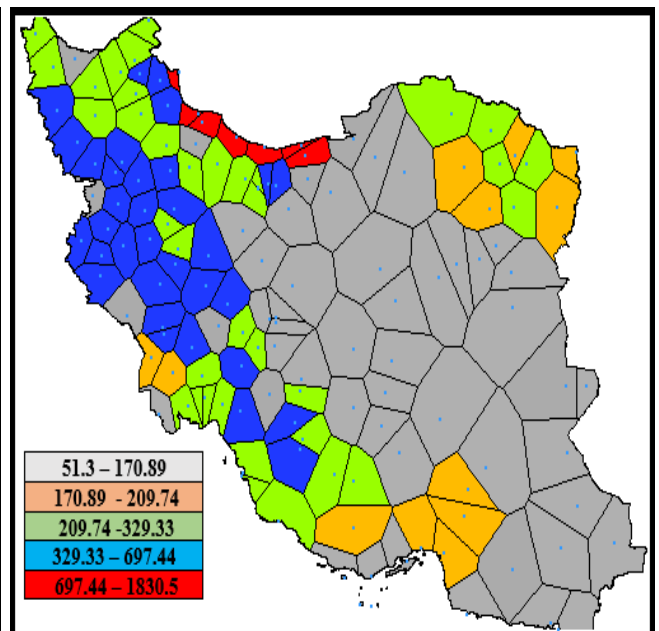
(1) Simple method.



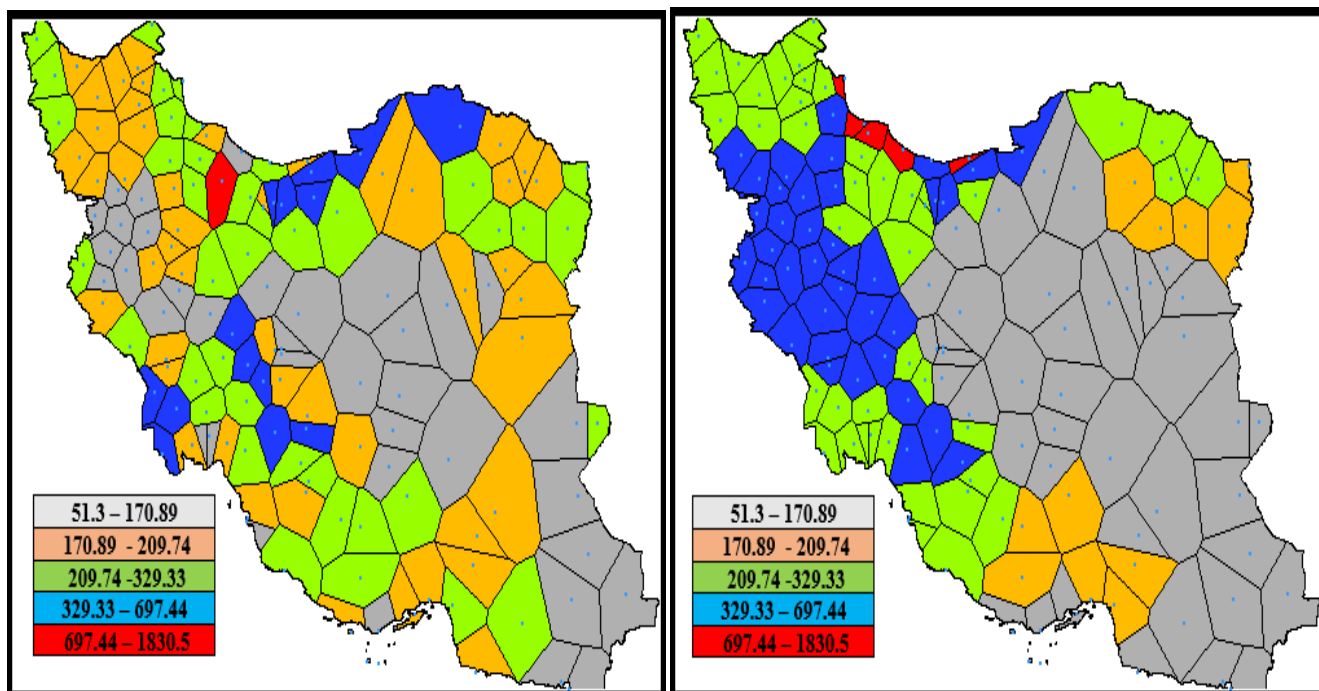
(2) Mean method.



(3) Mode method.

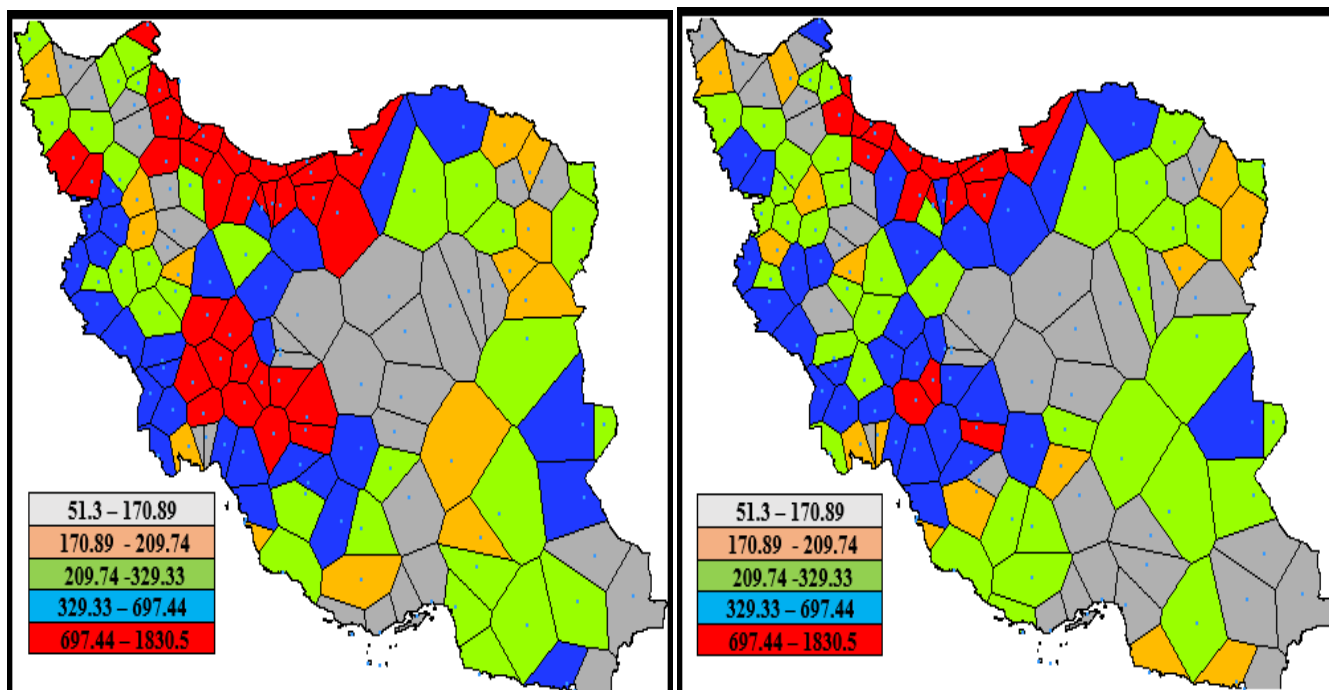


(4) Cluster method.



(5) Entropy method.

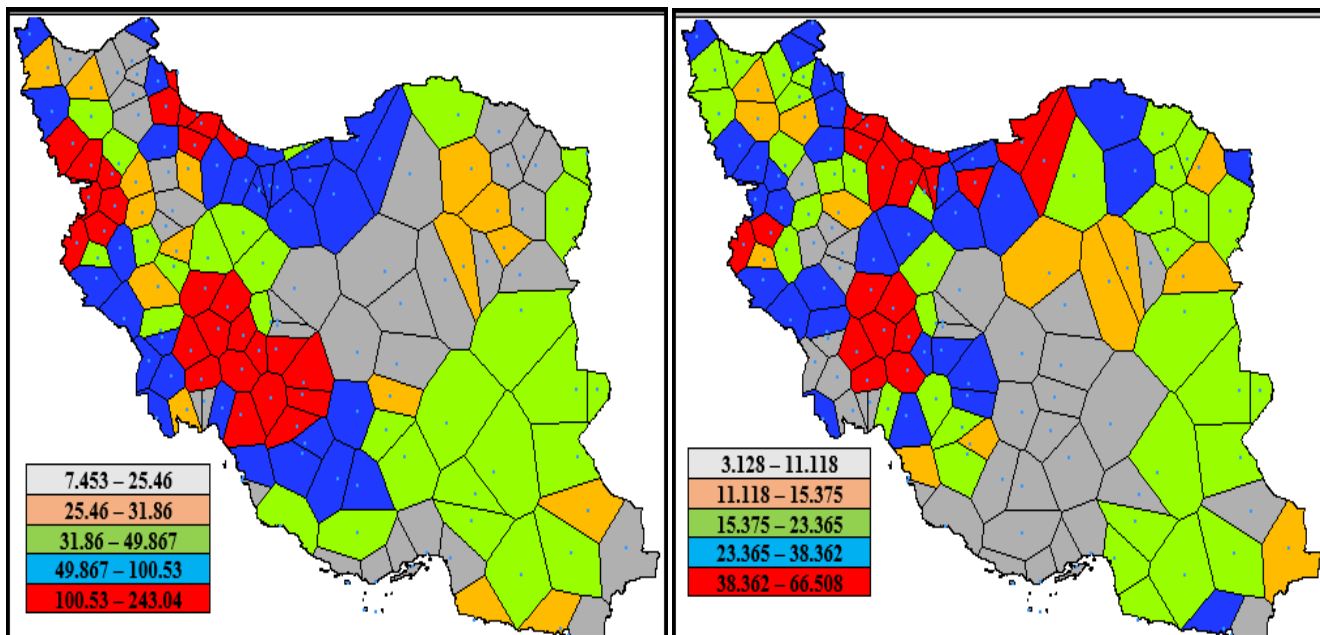
(6) Median method.



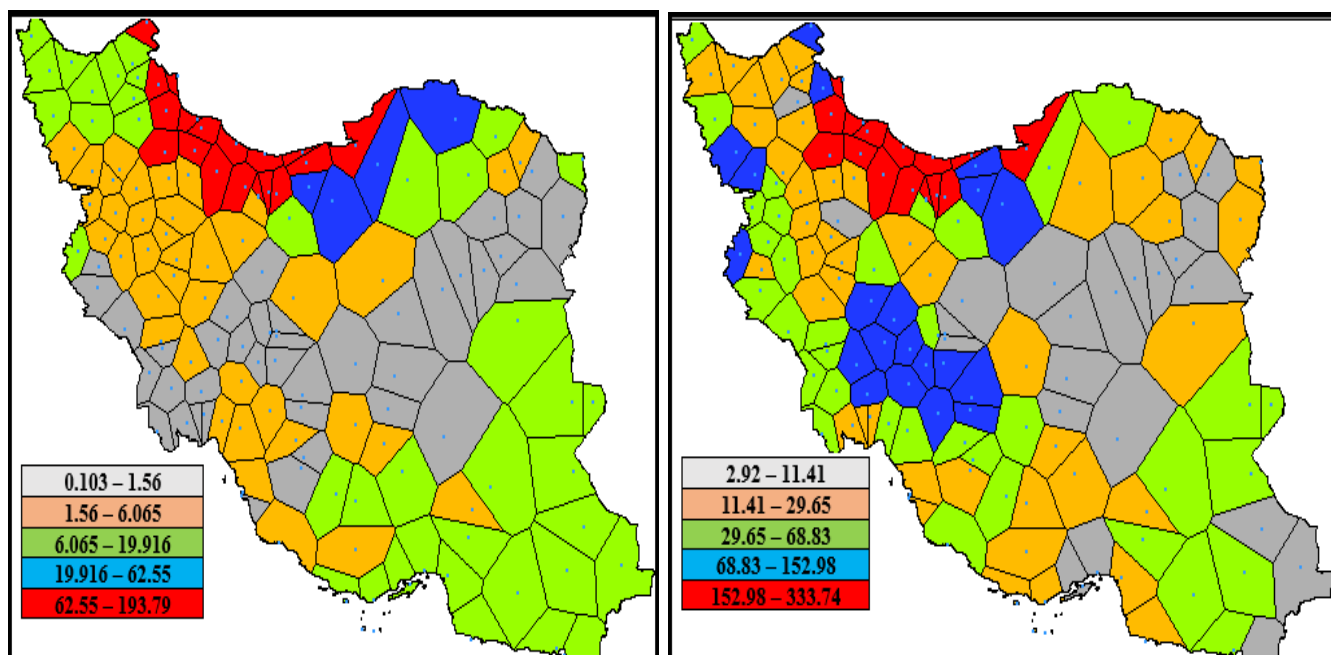
(7) Standard deviation method.

(8) IQR method.

Figure 4: Voronoi maps of annually precipitation data of simple (1) to simple (8) IQR methods.



(1) Winter precipitation (Standard deviation). (2) Spring precipitation (Standard deviation).



(3) Summer precipitation (Standard deviation). (4) Autumn precipitation (Standard deviation).

Figure 5: Voronoi maps of seasonal precipitation data of winter (1) to autumn (4) seasons.

stations in a specific subset of the plane. Voronoi polygons are created so that every location within a polygon is closer to the sample point in that polygon than any other sample point. As soon as the polygons are created, neighbors of a sample point are defined as any other sample point whose polygon shares a border with the chosen sample point [36]. The Voronoi diagram tool provides eight methods (simple, mean, mode, cluster, entropy, median, standard deviation and interquartile range) to assign or calculate values of precipitation for the polygons. Simple method, the value assigned to a polygon is the value recorded at the sample point within that polygon. Mean method, the value assigned to a polygon is the mean value that is calculated from the polygon and its neighbors. Mode method, all polygons are categorized using five class intervals. The value assigned to a polygon is the mode (most frequently) of the polygon and its neighbors. Cluster method, all polygons are categorized using five class intervals. If the class interval of a polygon is different from each of its neighbors, the polygon is colored gray and put into a sixth class to distinguish it from its neighbors. Entropy method, all polygons are categorized using five classes based on a natural grouping of data values. The value assigned to a

polygon is the entropy that is calculated from the polygon and its neighbors that is: $EM = -\sum P_i \times \log p_i$ Where P_i is the proportion of polygons that are assigned to each class. Median method, the value assigned to a polygon is the median value calculated from the frequency distribution of the polygon and its neighbors. Standard deviation method, the value assigned to a polygon that is calculated from the polygon and its neighbors. Interquartile range method, the first and third quartiles are calculated from the frequency distribution of a polygon and its neighbors [36]. This paper examines the Voronoi diagrams between annual and seasonal rainfall series in Iran for the period 1975-2014. At the geostatistical and spatial modeling of the climatic elements, we have to assume that the expected values of the variables are changing in temporal and in spatial alike. The spatial change means that the climate is different in the regions. Two trends were discovered in the precipitation. The red line projected against the XZ (North-South) plane represented a 2nd order trend. With a rotation angle of 110°, the trend stretched from the NNW to the S-SE. The blue line projected against the YZ plane at 45 is also a second order trend from the NE to the SW. Precipitation analysis revealed an upward trend in monthly rainfall, especially for the last 15 years of data range (1975-2014). We also explored the trends between each month's precipitations because primary analyses showed different trends within monthly precipitation. When analyzing, the trends of monthly precipitation and the rate of these variations were studied (Figure 6).

Exploration of Iran precipitation: Rainfall spatial variation exerts a considerable influence on the temporal-spatial distribution of state variables of a hydrological - climatic system. Its impact depends on factors such as various scales [19,60]. Several methods, such as semivariograms, autocorrelation, spatial statistical analysis and etc., are chosen to analyses and characterize spatial temporal characteristics of these rainfall variations [61]. In the study of geostatistical-spatial patterns, it is important that close observations are more likely to be similar than those spatial autocorrelation [30,62]. The spatial autocorrelation and correlation of precipitation are examined by the data correlation. To understand the spatial autocorrelation characteristics of regionalized rainfall at monthly, seasonal and annual scales, it was necessary to examine the impacts of separation distance on the model of such spatial autocorrelation [63]. The semivariogram/covariance cloud allows examining the spatial autocorrelation between the measured precipitations of stations. This tool examines the local characteristics of spatial autocorrelation contained in a rainfall database. The semivariogram/covariance cloud allows examining precipitation of stations' relationships. However, a certain distance is reached where the cloud flattens out; indicating that the values of the pairs of points separated by more than this distance are no longer correlated [52]. This study mainly implements semivariograms and spatial autocorrelation or the geostatistical-spatial statistical analysis. Looking at the Figure semivariogram, if it appears that some locations of precipitation stations that are close together (near zero on the x-axis) have a higher semivariogram value (high on the y-axis) than expected, you should investigate these pairs of locations to see if there is a possibility that the data is inaccurate. By estimating, spatial autocorrelation and semivariograms were identified based on the precipitation variations and the reconstructed correlation matrix was also identified based on the precipitation variations. Moreover, spatial relationships of the monthly precipitation were determined as standardized and non-standardized values were calculated. In the study of geostatistical - spatial patterns, it is important that close observations are more likely to be similar than those spatial autocorrelation. To assess the relative importance of precipitation spatial patterns variations, we compared standardized and non-standardized coefficients. By estimating semivariogram/covariance cloud of seasonal precipitation, the capability of each month in predicting the studied series was revealed. The seasonal precipitation semivariogram/covariance cloud allows examining the spatial autocorrelation between the measured precipitations of stations. This tool examines the local characteristics of spatial autocorrelation contained in a rainfall database (Figure 7).

Spatial modelling Iran monthly precipitation: Rainfall spatial variations exert a considerable influence on the temporal-spatial distribution of state variables of a hydrological - climatic system. Its impact depends on factors such as various scales. Several methods, such as inverse distance weighted, kriging and etc., are chosen to analyze and characterize spatial - temporal characteristics of these rainfall variations [61]. Modelling Iran monthly precipitation can be stated as follows:

Inverse Distance Weighting (IDW) interpolation: Inverse distance weighting (IDW) is an interpolation method that estimates precipitation values from a set of weighted sample points with measurement values [13,40]. IDW interpolation may be preferred over kriging technique when there is a problem of making meaningful estimates of the field spatial structure from sparse data [25,28,64]. In this paper it was two-fold. Firstly, we aimed to determine the geostatistics methods for rainfall data for application to countrywide climatic modelling in Iran. To investigate this, four different spatial interpolation methods were evaluated: inverse distance weighting (IDW) and kriging types. Secondly, we used spatial statistical methods to compare values of the forecasted precipitation variations at different stations [35,65,66]. The Geostatistical Wizard's neighborhood type is smooth with a maximum neighbors of 15, minimum neighbors of 10 and a l-sector search type. Detailed differences are seen in Fig 8. When the geostatistical model is optimized for monthly precipitation, the variations range of monthly precipitation becomes 688.73 mm in autumn to 195.981 mm in spring (Figure 8). The cross validation of IDW for seasonal precipitation values are as follows: 4.74 for autumn, 2.44 for summer, 0.558 for spring and 1.68 for winter respectively (Figure 8).

- Kriging and cokriging methods: Various geostatistical interpolation types can be obtained from the linear model by applying the generalized least-squares estimation for the expected values. The type of kriging method depends on the model assumed for the expected values. Kriging methods depend on mathematical and statistical models. Kriging assumes that at least some of the precipitation spatial variations observed in natural conditions can be modeled by random processes with spatial autocorrelation, and require that the spatial autocorrelation be explicitly modeled. The Kriging, a geostatistical interpolation technique, is a suitable and linear unbiased spatial interpolation type. The geostatistical analysis offers several types of kriging, which are suitable for different types of data and have different underlying assumptions: Ordinary, Simple, Universal, Indicator, Probability, Disjunctive and Empirical Bayesian. Ordinary kriging assumes the model: $Z(S) = \mu + \varepsilon(s)$. Where μ an unknown is constant, $\varepsilon(s)$ is error and trend, with $\mu(s)$ changing with s , where x, y are the variables for the x-latitude and y-longitude, respectively, z is statistically analyzed from data. One of the main issues concerning ordinary kriging is whether the assumption of a constant mean is reasonable. Ordinary kriging can use either semivariograms or covariance, use transformations and remove trends, and allow measurement error. Simple kriging assumes this model: $Z(S) = \mu + \varepsilon(s)$ Where μ is a known constant. Universal kriging assumes the model: $Z(S) = \mu(s) + \varepsilon(s)$ Where $\mu(s)$ is some deterministic function (\cdot). A second-order polynomial is the trend long dashed line-which is $\mu(s)$. If you subtract the second-order polynomial from

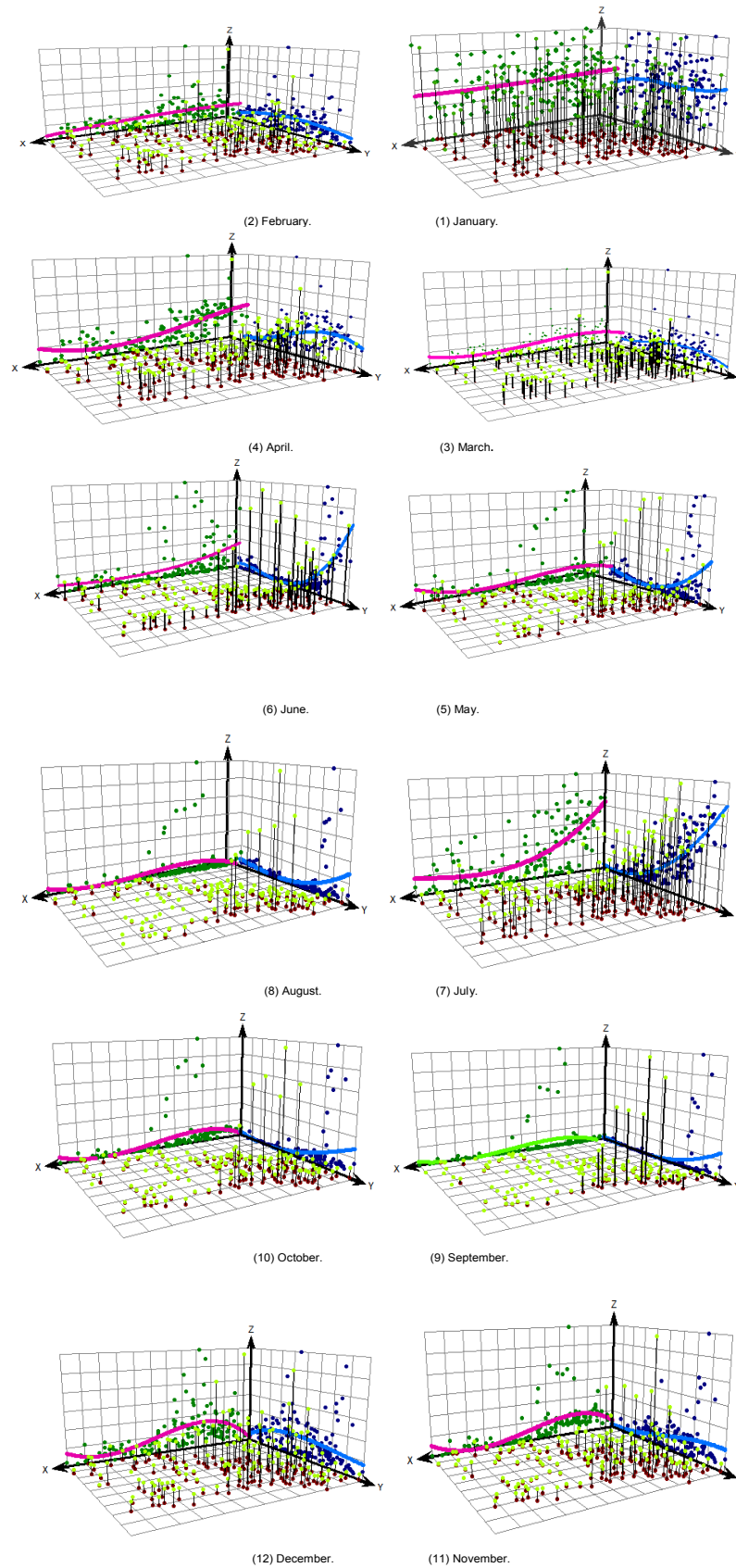
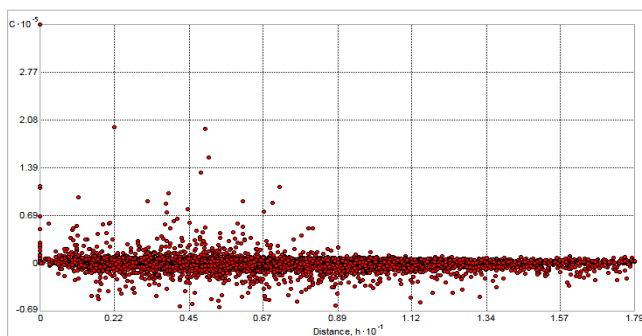
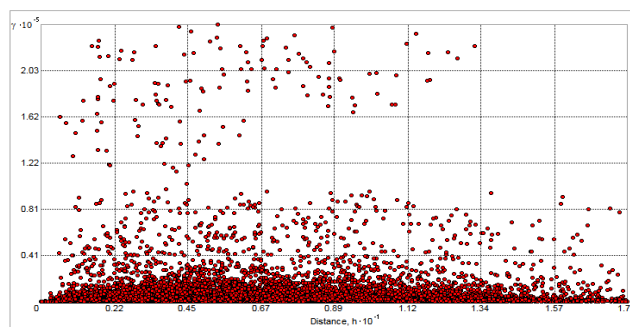


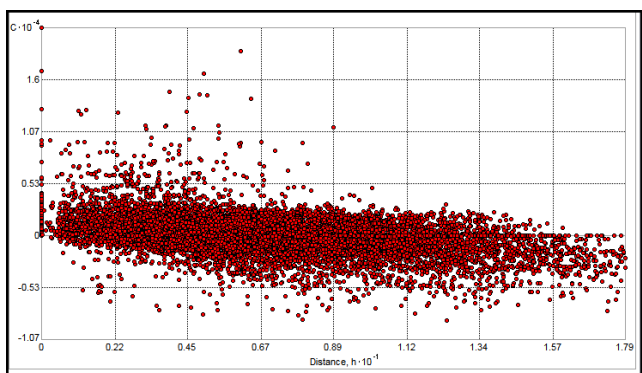
Figure 6: Trend analyses of monthly precipitation data of January (1) to December (12) by three dimensional plots of the dataset from 140 climate stations over Iran. Monthly precipitation values are projected onto the x-z (west) and y-z (north) planes of the scatter plots, respectively.



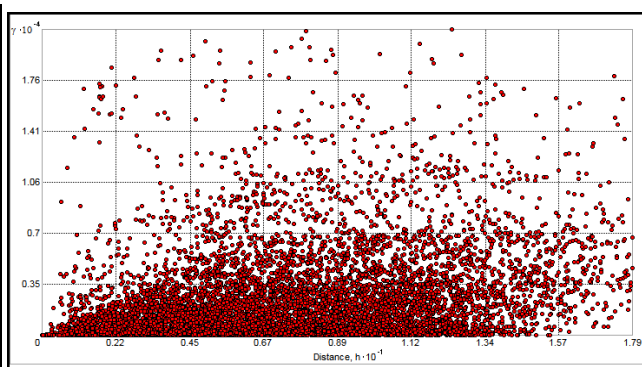
(b) Covariance of winter precipitation.



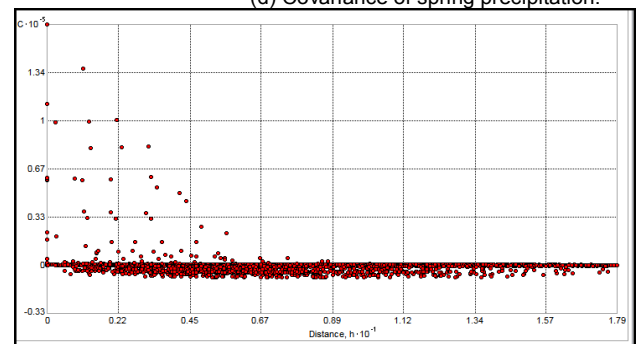
(a) Semivariogram of winter precipitation.



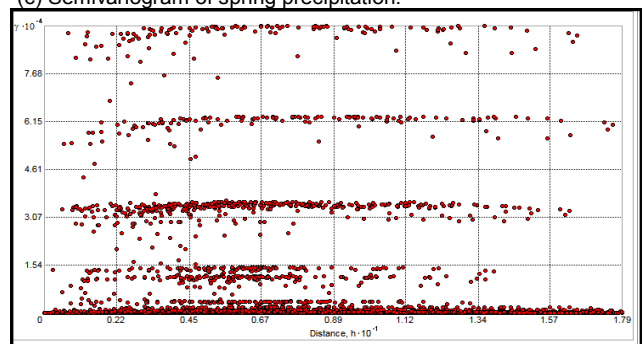
(d) Covariance of spring precipitation.



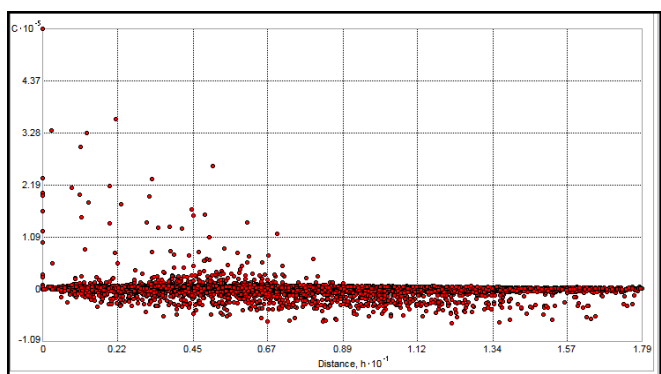
(c) Semivariogram of spring precipitation.



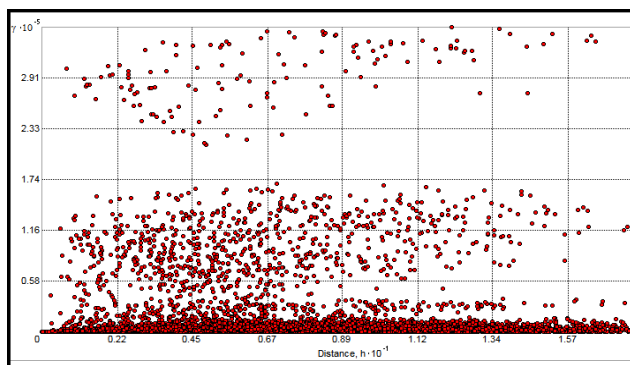
(f) Covariance of summer precipitation.



(e) Semivariogram of summer precipitation.

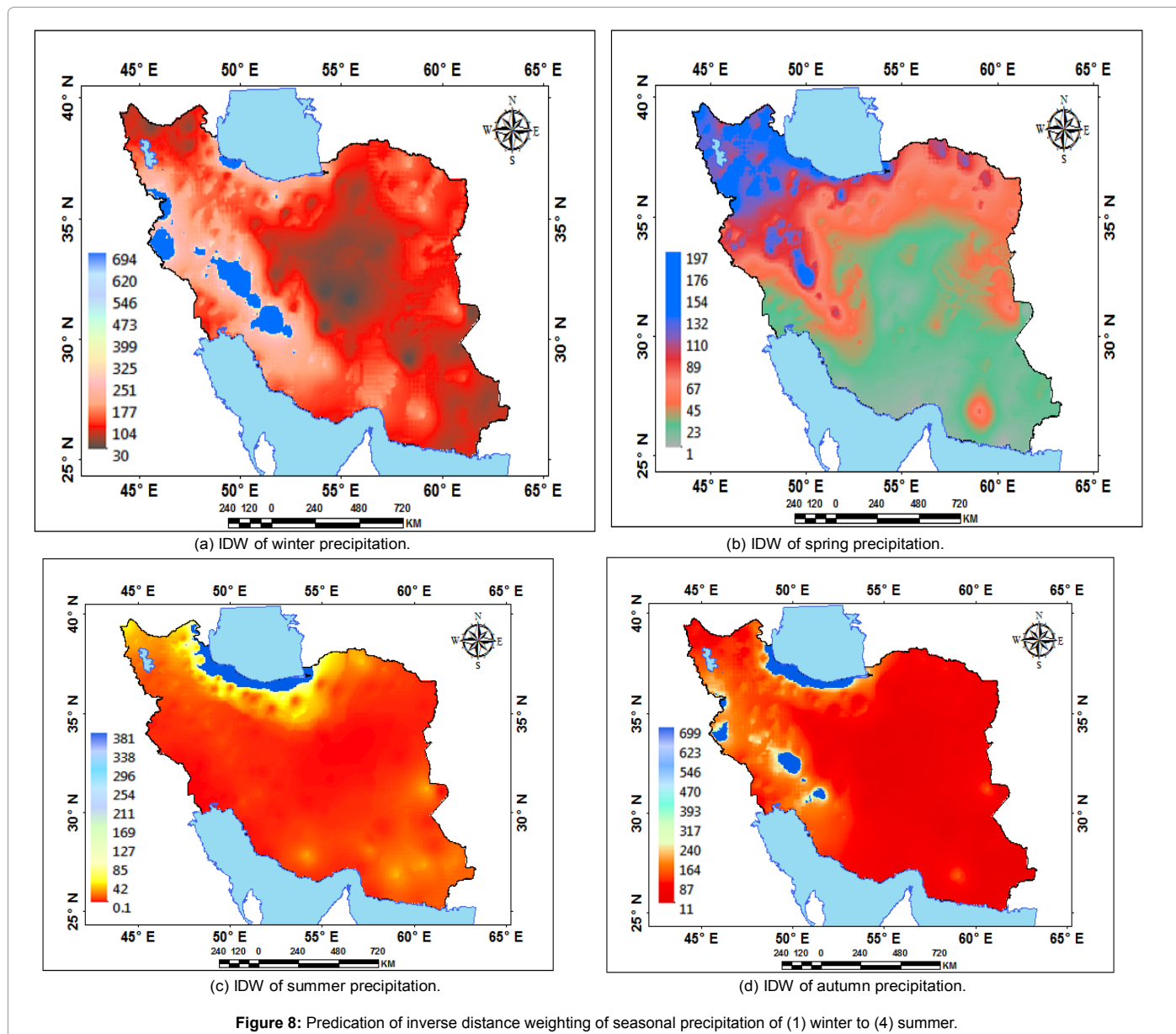


(h) Covariance of autumn precipitation.



(g) Semi-variogram of autumn precipitation.

Figure 7: Covariance / semi-variogram of seasonal precipitation data of winter (1) to autumn (4).



the original data, you obtain the errors, $\varepsilon(s)$ which is assumed to be random. Indicator kriging assumes the model: $I(S) = \mu + \varepsilon(s)$ Where μ is an unknown constant and $I(s)$ is a binary variable. Indicator kriging can use either semivariograms or covariance, which are the mathematical forms you use to express autocorrelation. Probability kriging assumes the model:

$f I(S) = I[Z(S) > c_t] = \mu_1 + \varepsilon_1(s), Z(S) = \mu_2 + \varepsilon_2(S)$ Where μ_1 and μ_2 are unknown constants and $I(s)$ is a binary variable created by using a threshold indicator, $1(Z(s) > c_t)$. Notice that now there are two types of random errors, $\varepsilon_1(s)$ and $\varepsilon_2(s)$ so there is autocorrelation for each of them and cross-correlation between them. Probability kriging strives to do the same thing as indicator kriging, but it uses cokriging in an attempt to do a better work. Disjunctive kriging assumes the model: $f[Z(S)] = \mu_1 + \varepsilon(s)$, where μ_1 is an unknown constant and $f(Z(s))$ is an arbitrary function of $Z(s)$. Notice that you can write $f(Z(S)) = I(z(s) > c_t)$, so indicator kriging is a special case of disjunctive kriging. In Geostatistical Analyst, you can predict either the value itself or an indicator with disjunctive kriging. Empirical Bayesian kriging (EBK) is a geostatistical interpolation method that automates the most difficult aspects of building a valid kriging model [36,67]. Other kriging methods in Geostatistical Analyst require to manually adjusting parameters to receive accurate results, but EBK automatically calculates these parameters through a process of sub setting and simulations. Empirical Bayesian kriging also differs from other kriging methods by accounting for the error introduced by estimating the underlying semivariogram. In EBK, it's possible to analyze the empirical distribution of the parameter estimates because many semivariograms are estimated at each location. In this section, we present the application of kriging spatial interpolation methods for precipitation. This spatial interpolation is applied to monthly and seasonal precipitation variables independently. For simplicity, meteorological variable method is used to indicate either the precipitation variable [53,60].

There are several components of geostatistical models. The most important ones are examining the data through exploratory spatial data

analysis (ESDA) and variography, building a kriging model to suit precipitation variations and check that the results are accurate by performing cross validation and validation and comparing alternate models to choose the best. There are different types of semivariogram / covariance models. Geostatistical Analyst provides the following functions to model the empirical semivariogram (kriging): Circular, Spherical, Tetraspherical, Pentaspherical, Exponential, Gaussian, Rational Quadratic, Hole Effect, K-Bessel, J-Bessel and Stable. The selected model influences the prediction of the precipitation values, particularly when the curve shape near the origin differs significantly. The steeper the curve nears the origin, the more influence the closest neighbors will have on the prediction. Semivariogram/Covariance modeling is a key step between spatial description and spatial prediction.

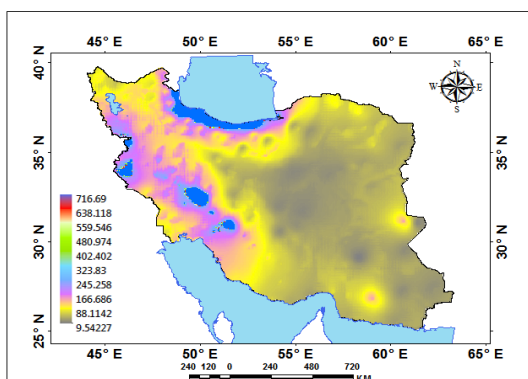
The main application of geostatistics is the prediction of attribute values at unsampled locations (kriging). The process of modeling semivariograms and covariance functions fits a semivariogram or covariance curve for precipitation data. The goal is to achieve the best fit, and also incorporate your knowledge of the precipitation variations in the model. The model will then be used in precipitation predictions. When fitting a model, explore for directional autocorrelation in precipitation. The sill, range, and nugget are the important characteristics of the model. In spatial modeling of the semivariogram, we begin with a graph of the empirical semivariogram, computed as: $SV(\text{distance}) = 0.5 \times \text{average} [V_i - V_j]^2$, where V_i is value at location and V_j is value at location [36]. Various methods of kriging and cokriging have been used. In this study, geostatistical methods (kriging and cokriging include: Ordinary, simple, universal, indicator, probability, disjunctive and empirical Bayesian) was applied on the monthly and seasonal precipitation to investigate their precision on mapping the precipitation variations (Figure 9).

Average nearest neighbor: The average nearest neighbor tool returns five values: observed mean distance, expected mean distance, nearest neighbor index, z-score, and p-value [36,68,69]. The z score and p-value results are measures of statistical significance which tell you whether or not to reject the null hypothesis. The p-value is a probability. For the pattern analysis tools, it is the probability that the observed spatial pattern was created by some random processes [27,70]. When the p-value is very small, it means it is very unlikely (small probability) that the observed spatial pattern is the result of random processes, so the null hypothesis can be rejected. When you run a feature pattern analysis tool and it yields small p-values and either a very high or a very low z-score, this indicates it is unlikely that the observed spatial pattern reflects the theoretical random pattern represented by your null hypothesis. The critical z-score values when using a 95 percent confidence level are -1.96 and + 1.96 standard deviations. The uncorrected p-value associated with a 95 percent confidence level is 0.05. If your z-score is between -1.96 and + 1.96, your uncorrected p-value will be larger than 0.05, and you cannot reject the null hypothesis because the pattern exhibited could very likely be the result of random spatial processes. Several statistics in the Spatial Statistics toolbox are inferential spatial pattern analysis techniques including Spatial Autocorrelation (Global Moran's I), Cluster and Outlier Analysis (Anselin Local Moran's I), and Hot Spot Analysis (Getis-Ord Gi). A positive value for I indicates that a feature has neighboring features with similarly high or low attributes values; this feature is part of a cluster. A negative value for I indicates that a feature has neighboring features with dissimilar values; this feature is an outlier. However, the positive results of Moran's I statistic with significant p-values and high Z-scores indicate spatially clustered data sets. At the same time, negative Moran's I depicts that the spatial pattern is more spatially dispersed [30,36]. The average nearest neighbor used in relation to the stations chosen is spread evenly over the Iran. If the z-score is less than 1, the stations are clustered. Otherwise, the stations are generally spread (random) (Figure 10). The Spatial Autocorrelation (Global Moran's I) tool measures spatial autocorrelation based on both feature locations and feature values simultaneously. Given a set of features and an associated attribute, it evaluates whether the pattern expressed is clustered, dispersed, or random [36]. The Spatial Autocorrelation (Global Moran's I) was used in relation to the stations chosen spread evenly over the Iran (Figure 10).

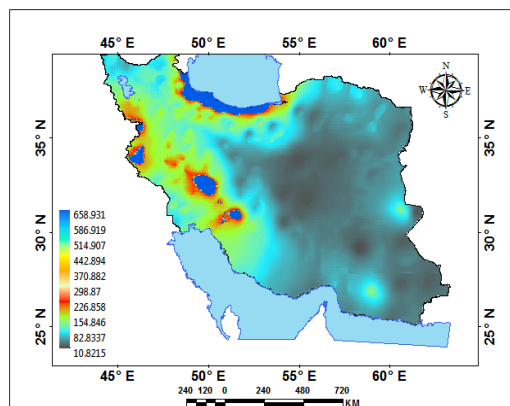
High/low clustering (Getis-Ord General G): The term hot spot has become an integral part of the study called data analysis and is popular with most of the analyst. A hot spot as the name suggests is a state of indicating some subjects of clusters in a spatial distribution [57,71]. The cluster/outlier type field distinguishes between a statistically significant cluster of high values (HH), cluster of low values (LL), outlier in which a high value is surrounded primarily by low values (HL), and outlier in which a low value is surrounded primarily by high values (LH). Statistical significance is set at the 95 percent confidence level. For statistically significant positive z-scores, the larger the z-score, the more intense the clustering of high values (hot spot) [13,72].

For statistically significant negative z-scores, the smaller the z-score, the more intense the clustering of low values (cold spot). In studying differences between properties in hotspot and cold spot values relative to values that were neither, no clear pattern emerged for predicting properties in cold spot values, suggesting that the examined factors may not be the most relevant predictors [71,73]. We applied cluster mapping methods to estimate the rate of similarity between precipitation values of adjacent stations. We used Getis-Ord general G-statistic to estimate the magnitude of clustering among stations. Both procedures estimate the spatial distribution of stations and determine the rate of similarity between adjacent station precipitation values. The Getis-Ord General G is capable of indicating the presence of hot spots or cold spots over the entire study area. Spatial clustering methods in climate, as previously explained, often apply spatially clustering, a process in which a spatial multivariate clustering methods are modified by introducing spatial patterns. The monthly precipitation combined was used in the computation of the Getis-Ord General G to select the suitable number of clusters. Based on the Gi method, statistically significant local clustering is indicated for both high values and low values in the study area for monthly precipitation. In Figure 11, Getis-Ord General G denote statistically significant spatial clusters of high values (hot-spots), spatial clusters of low values (cold-spots) and dots are not considered as significant, i.e., random distribution with no spatial clustering of either high or low values for seasonal precipitation.

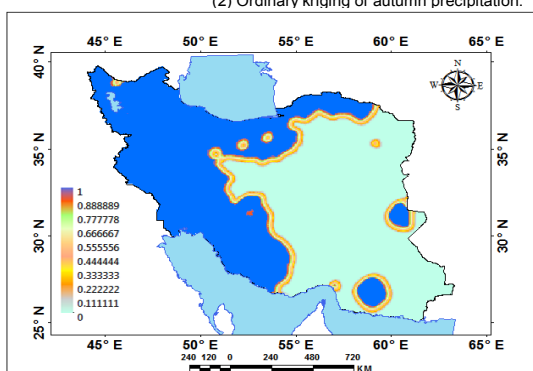
Multi-distance spatial cluster analysis (Ripley's K function): The Multi-distance spatial cluster analysis tool, based on Ripley's K-function, is another way to analyze the spatial pattern of incident point data. It summarizes the spatial dependence over a range of distances. The precipitation was examined by fitting linear models; the latter, by comparing Ripley's K function values to those expected under complete spatial randomness. Multi-distance spatial cluster analysis (Ripley's K function) tests whether precipitation associated with stations exhibit statistically significant clustering or dispersion across a range of distances [46,74]. This analysis produces expected and observed K values that the expected K value exceeds the observed K value for a particular distance, the distribution is more clustered than dispersed at the scale of the analysis (Figures 12 and 13).



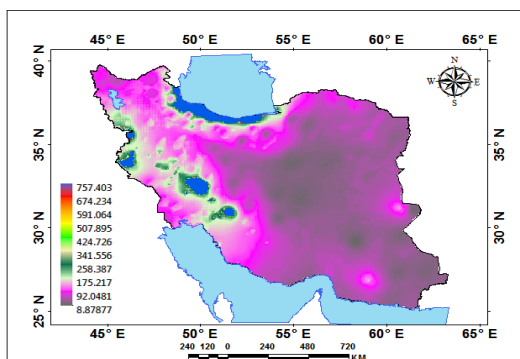
(2) Ordinary kriging of autumn precipitation.



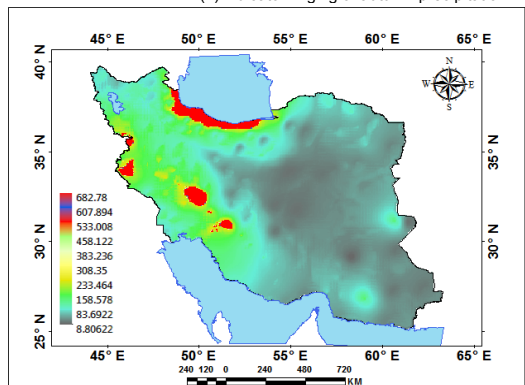
(1) Simple kriging of autumn precipitation.



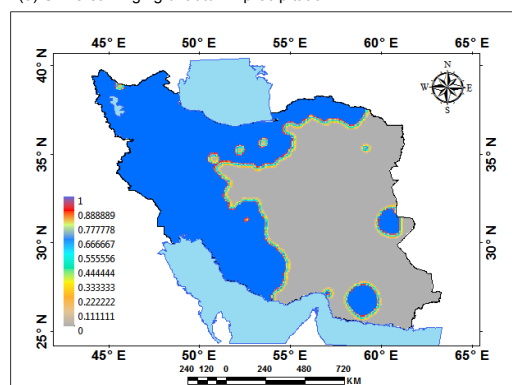
(4) Indicator kriging of autumn precipitation.



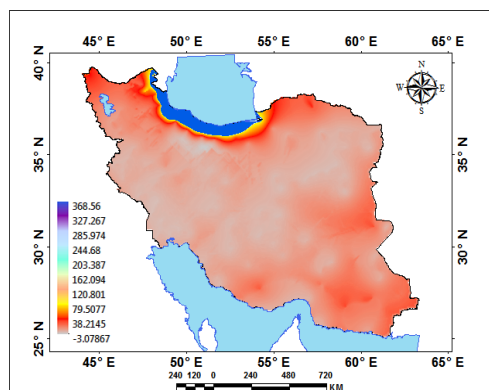
(3) Universal kriging of autumn precipitation.



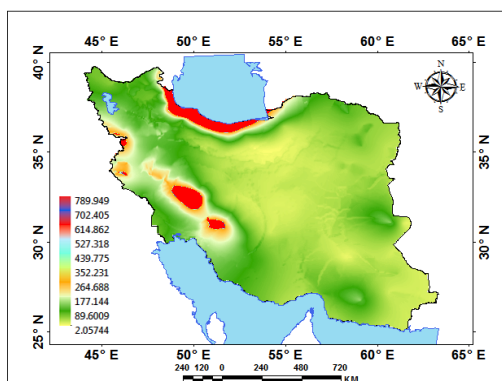
(6) Disjunctive kriging of autumn precipitation.



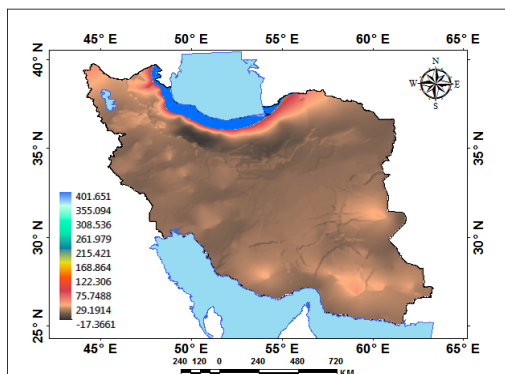
(5) Probability kriging of autumn precipitation.



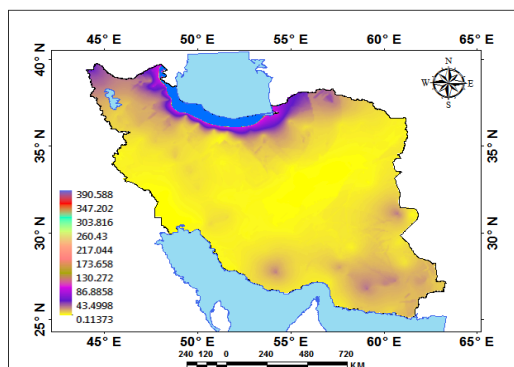
(8) Simple kriging of summer precipitation.



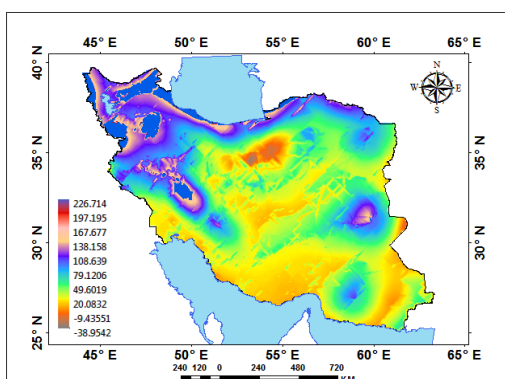
(7) Empirical bayesian kriging of autumn precipitation.



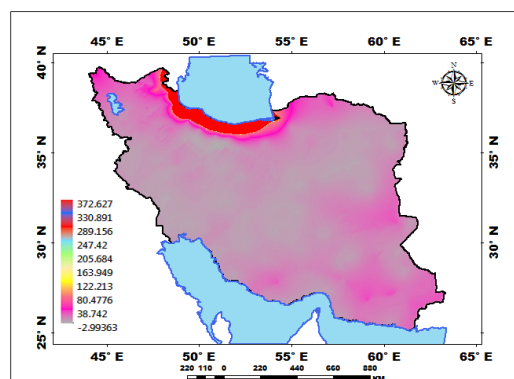
(10) Empirical bayesian kriging of summer precipitation.



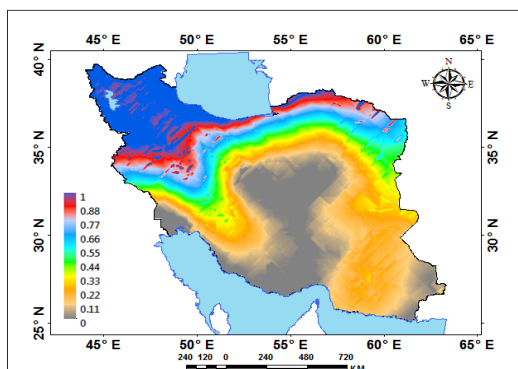
(9) Ordinary kriging of summer precipitation.



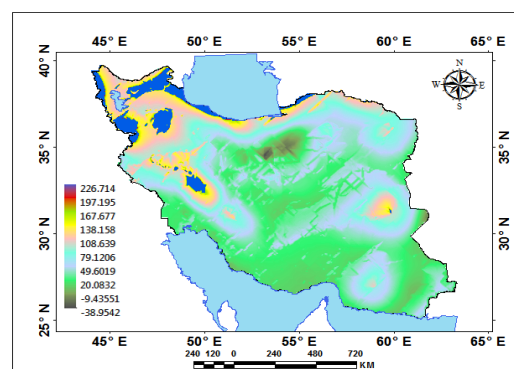
(11) Disjunctive kriging of summer precipitation.



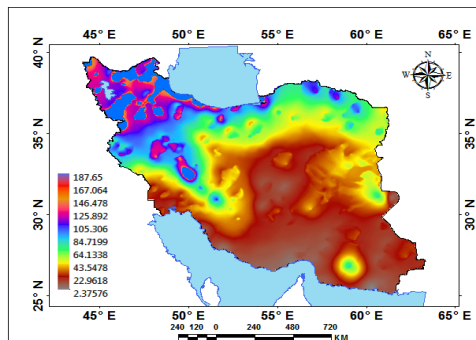
(12) Ordinary kriging of spring precipitation.



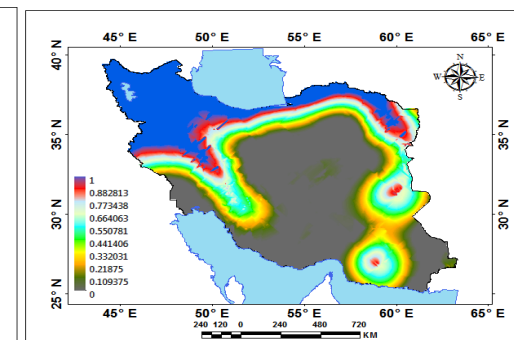
(14) Probability kriging of spring precipitation.



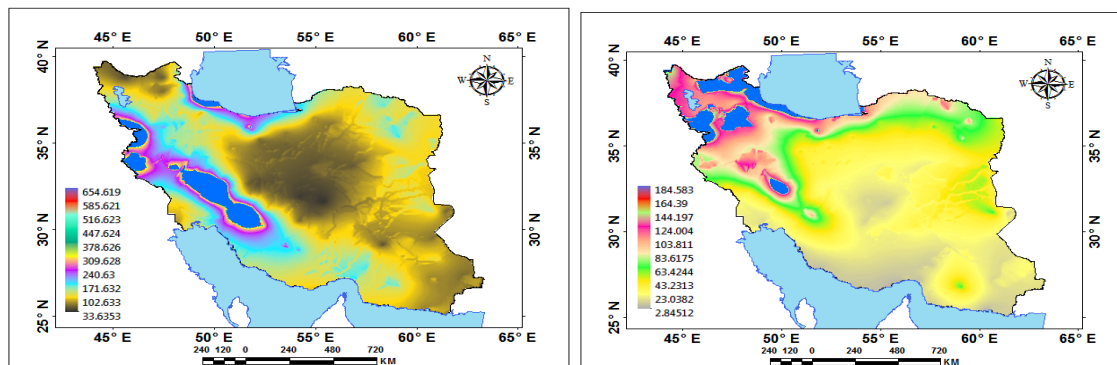
(13) Universal kriging of spring precipitation.



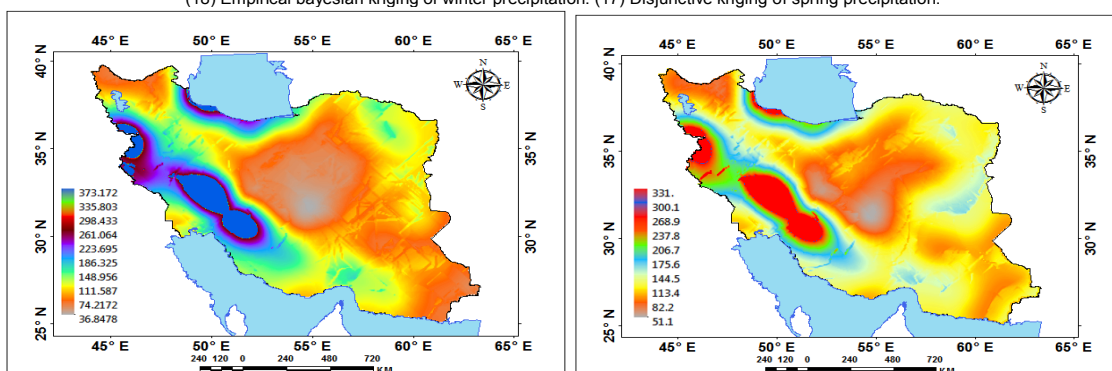
(16) Empirical bayesian kriging of spring precipitation.



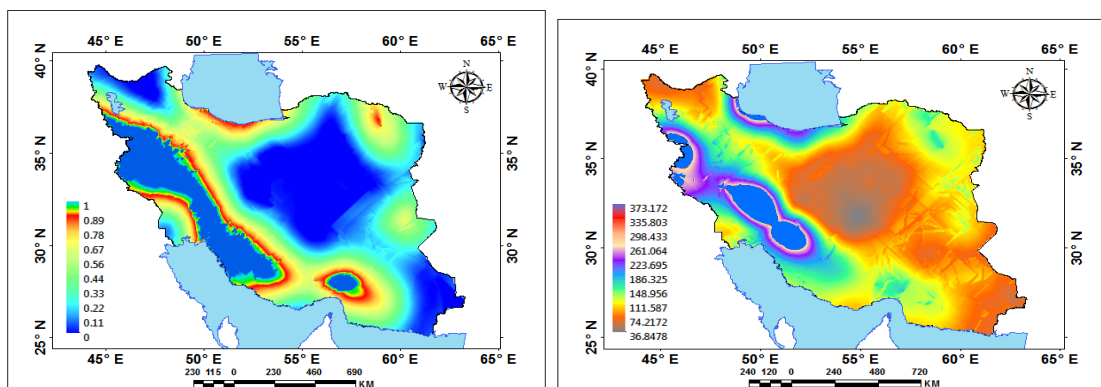
(15) Indicator kriging of spring precipitation.



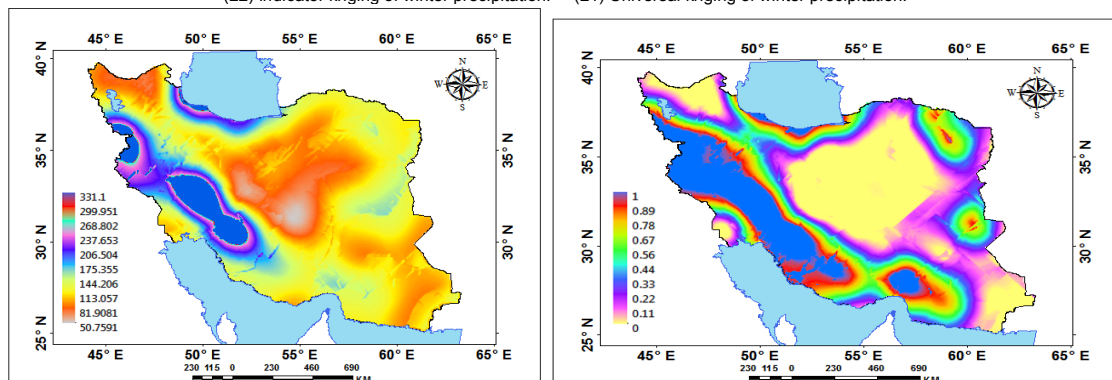
(18) Empirical bayesian kriging of winter precipitation. (17) Disjunctive kriging of spring precipitation.



(20) Ordinary kriging of winter precipitation. (19) Simple kriging of winter precipitation.

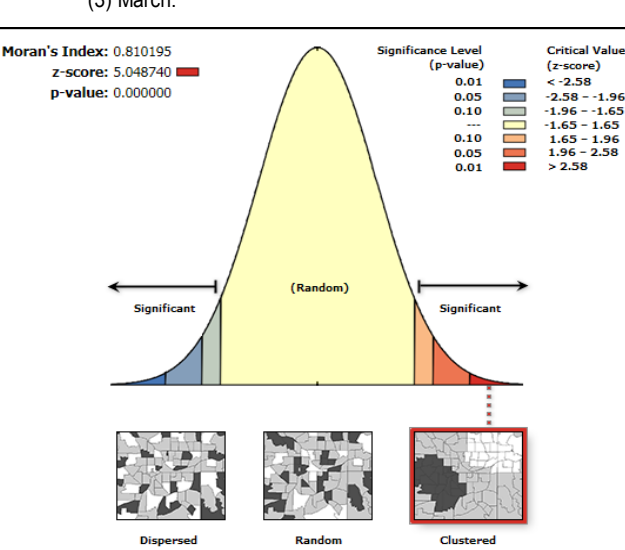
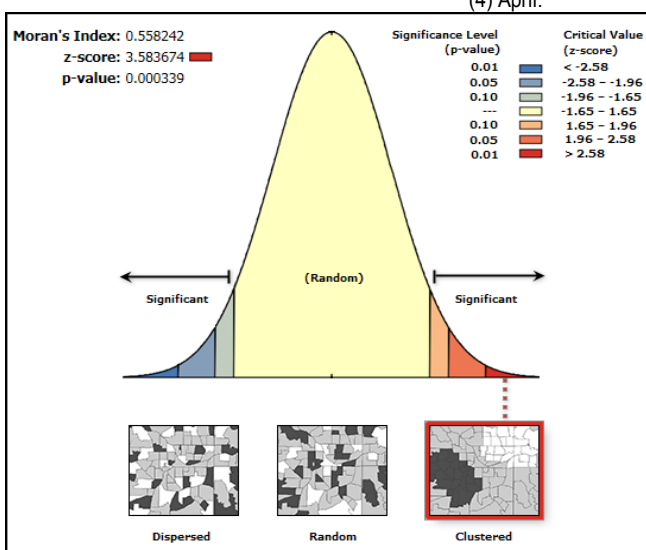
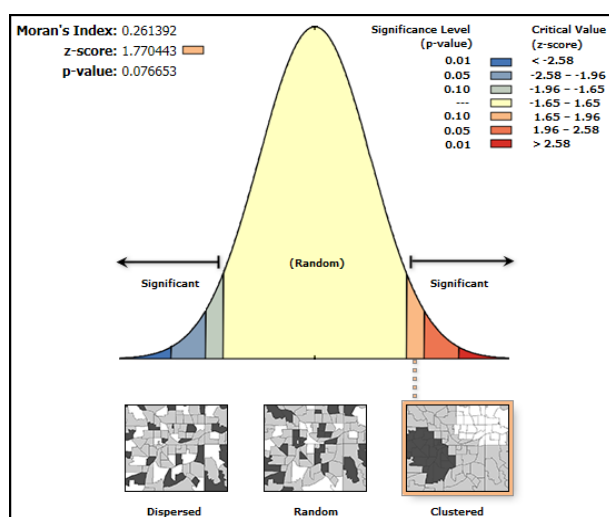
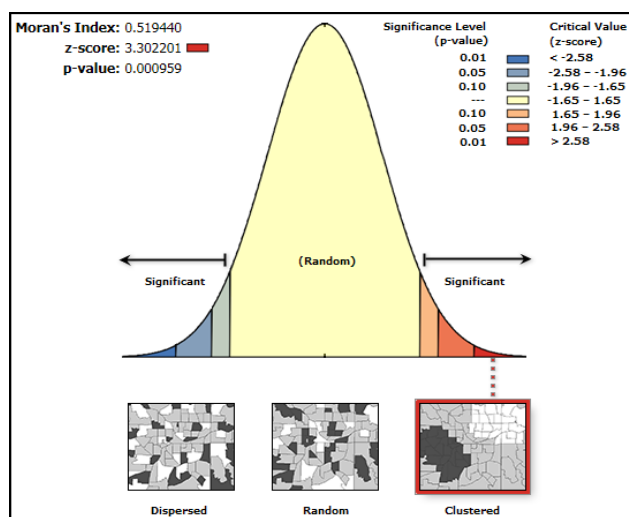
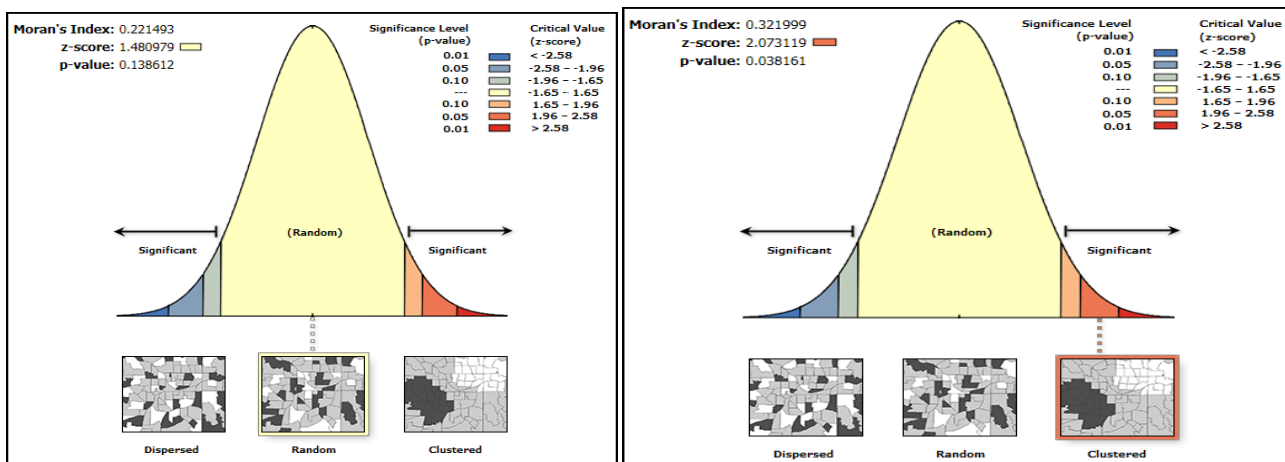


(22) Indicator kriging of winter precipitation. (21) Universal kriging of winter precipitation.



(24) Disjunctive kriging of winter precipitation. (23) Probability kriging of winter precipitation.

Figure 9: Kriging prediction of seasonal precipitation of (1) autumn to (24) winter.



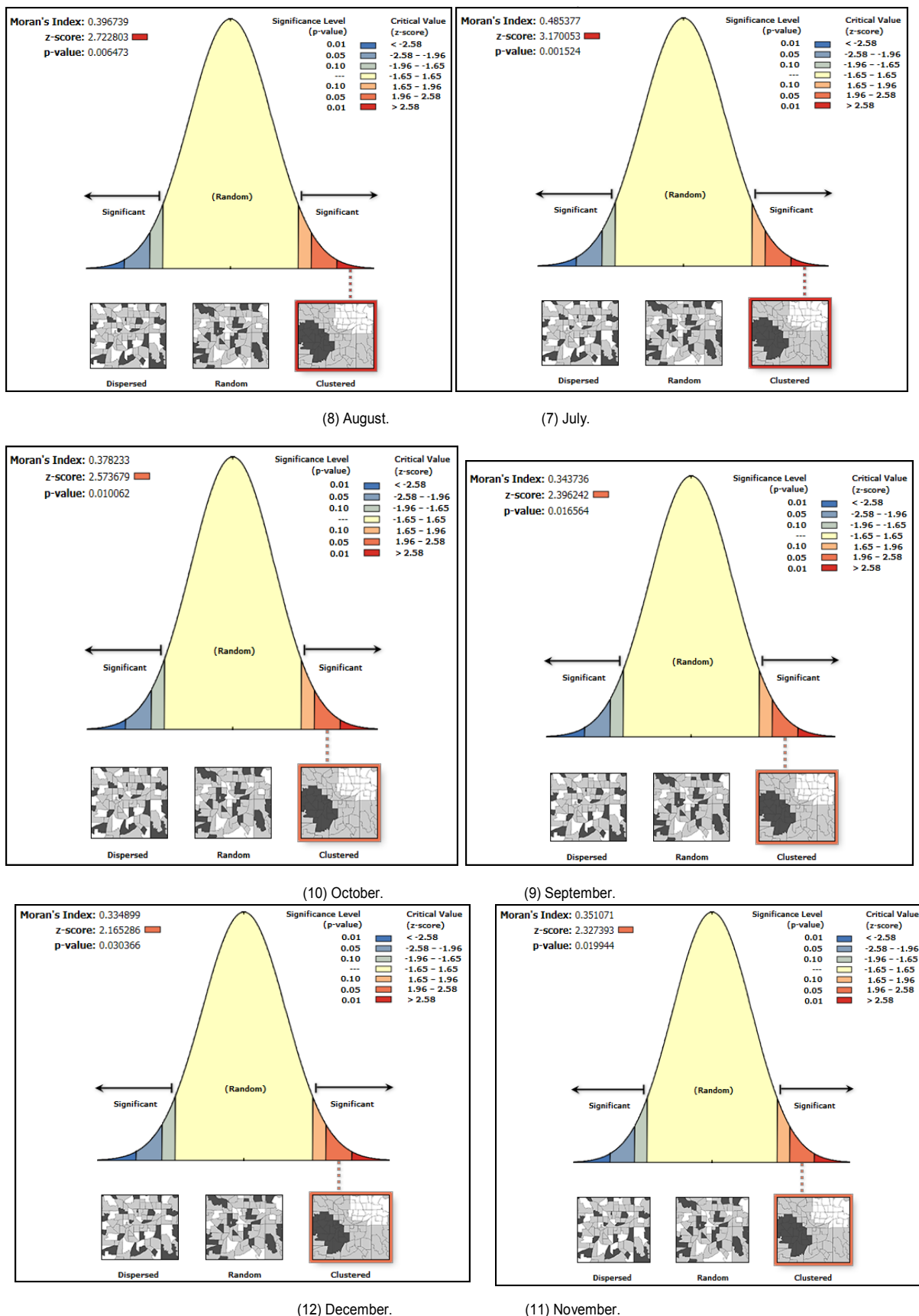
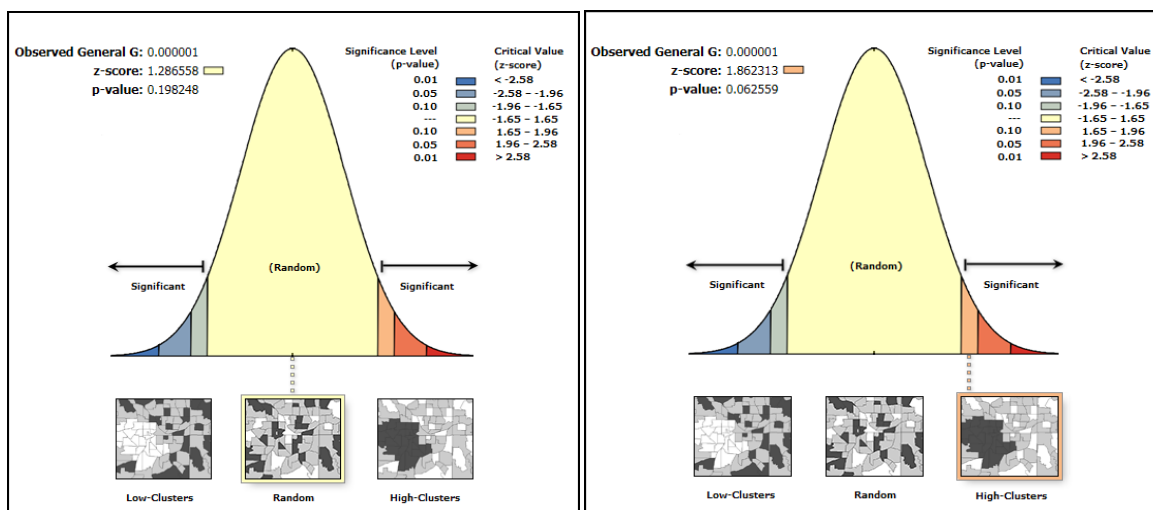
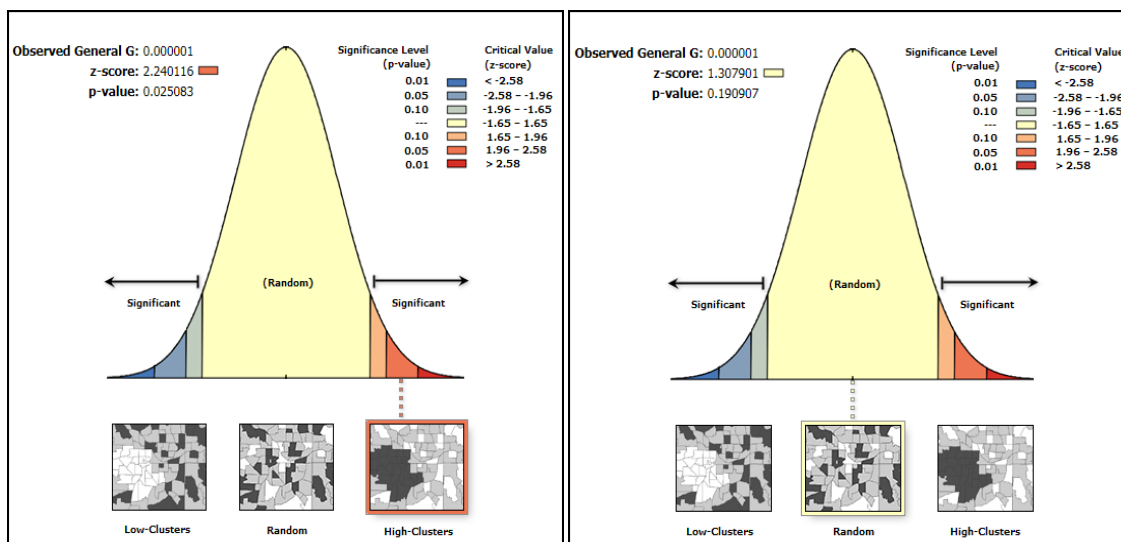


Figure 10: Average nearest neighbor and global Moran's index of monthly precipitation of (1) January to (12) December.



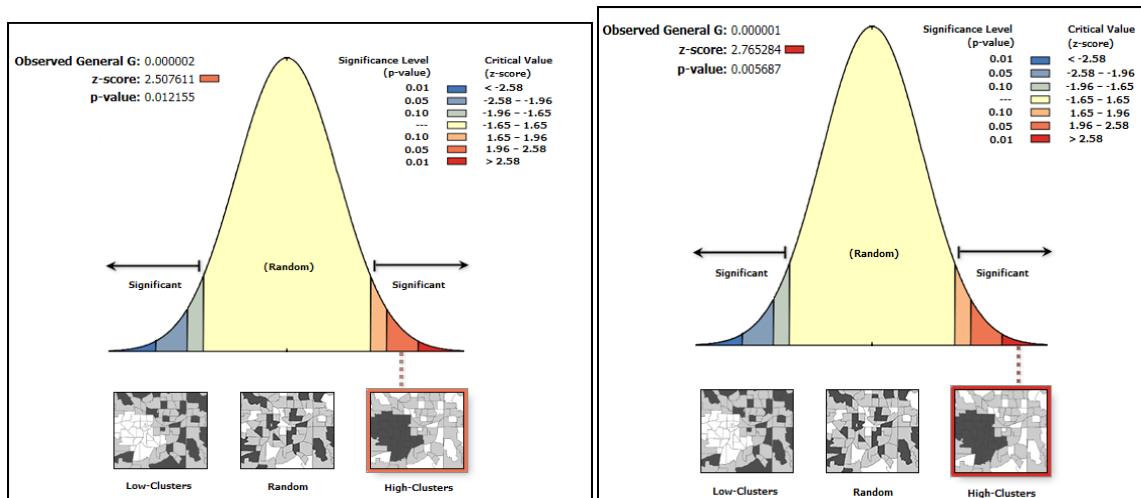
(2) High/low clustering of February.

(1) High/low clustering of January.



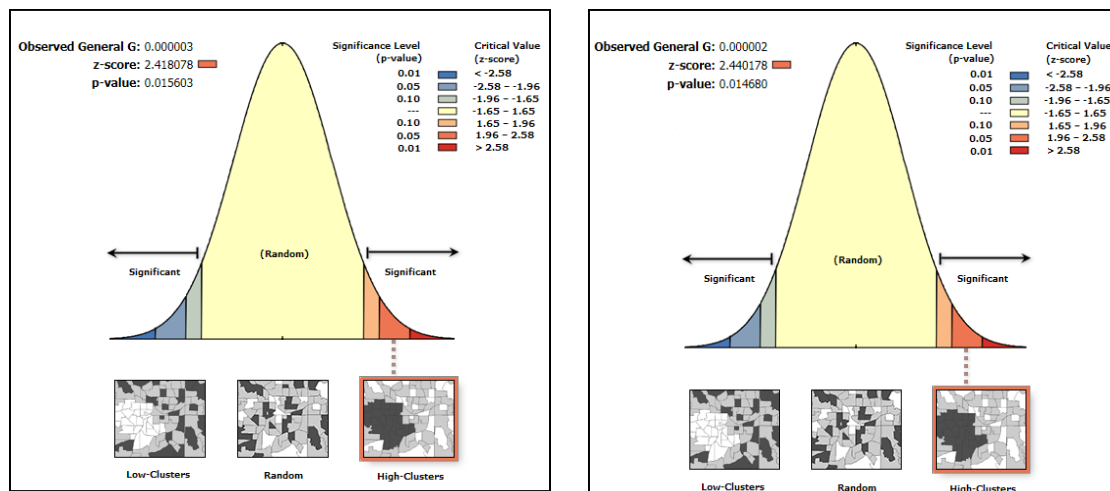
(4) High/low clustering of April.

(3) High/low clustering of March.



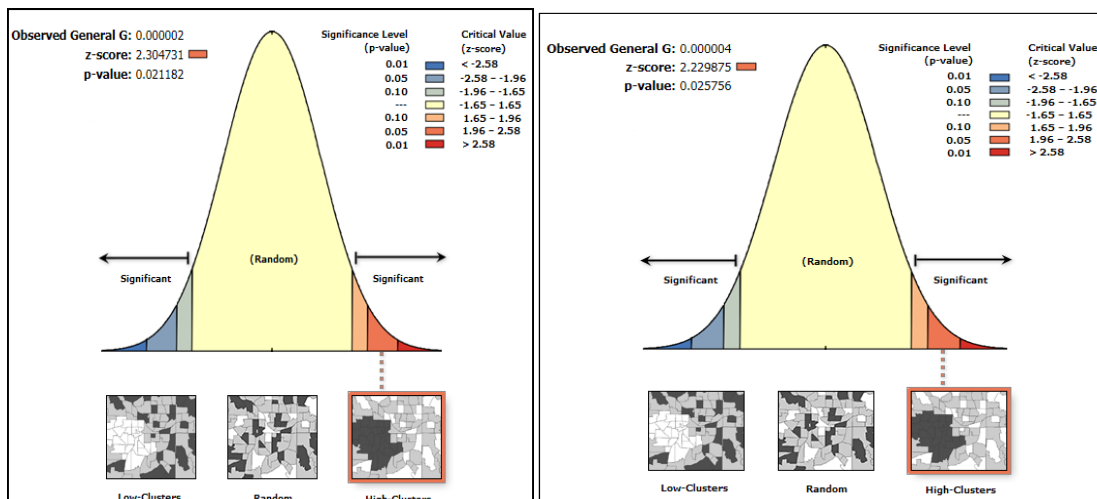
(6) High/low clustering of June.

(5) High/low clustering of May.



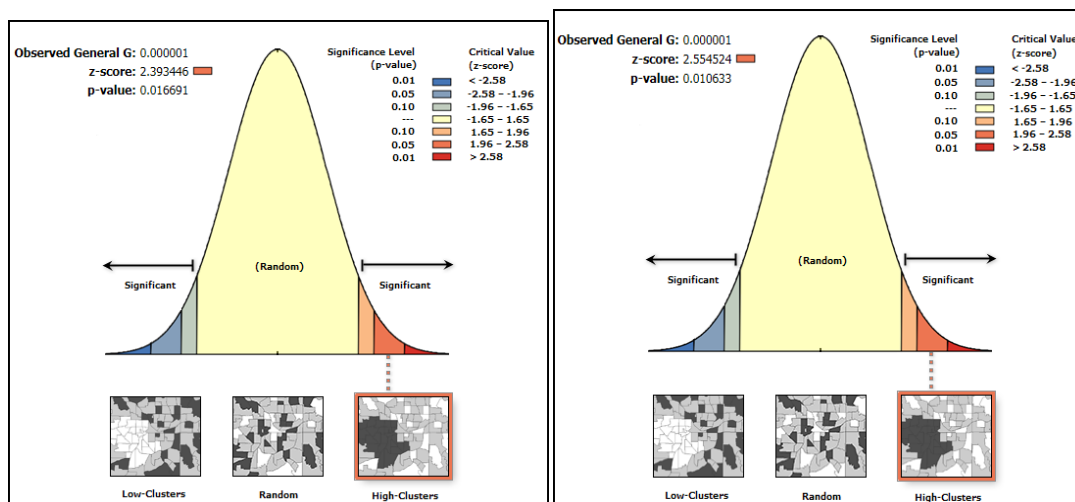
(8) High/low clustering of August.

(7) High/low clustering of July.



(10) High/low clustering of October.

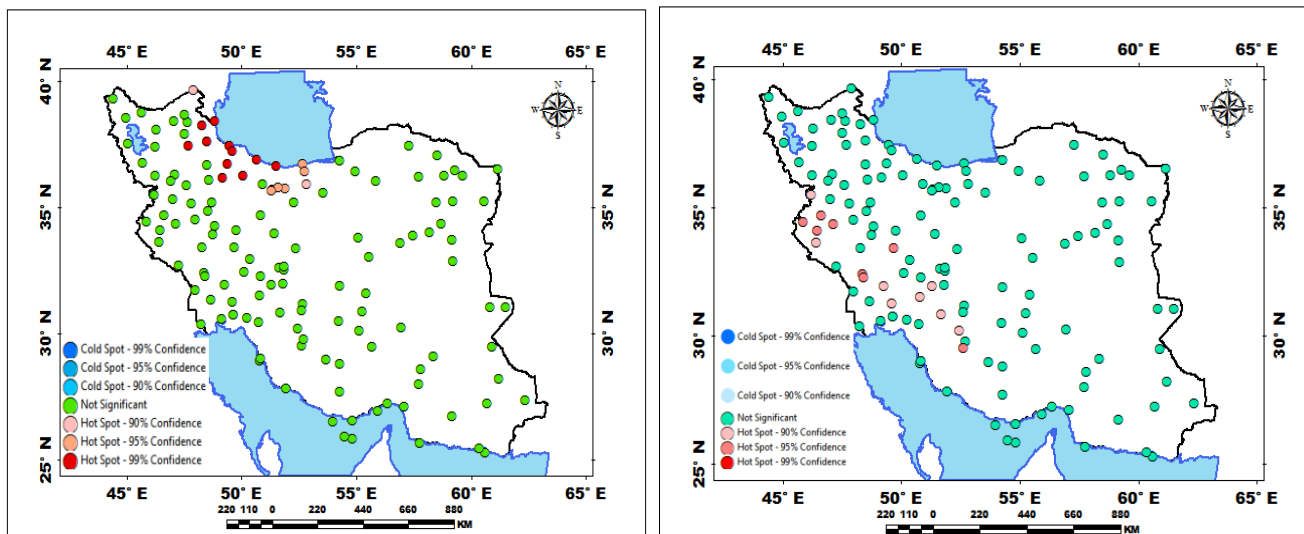
(9) High/low clustering of September.



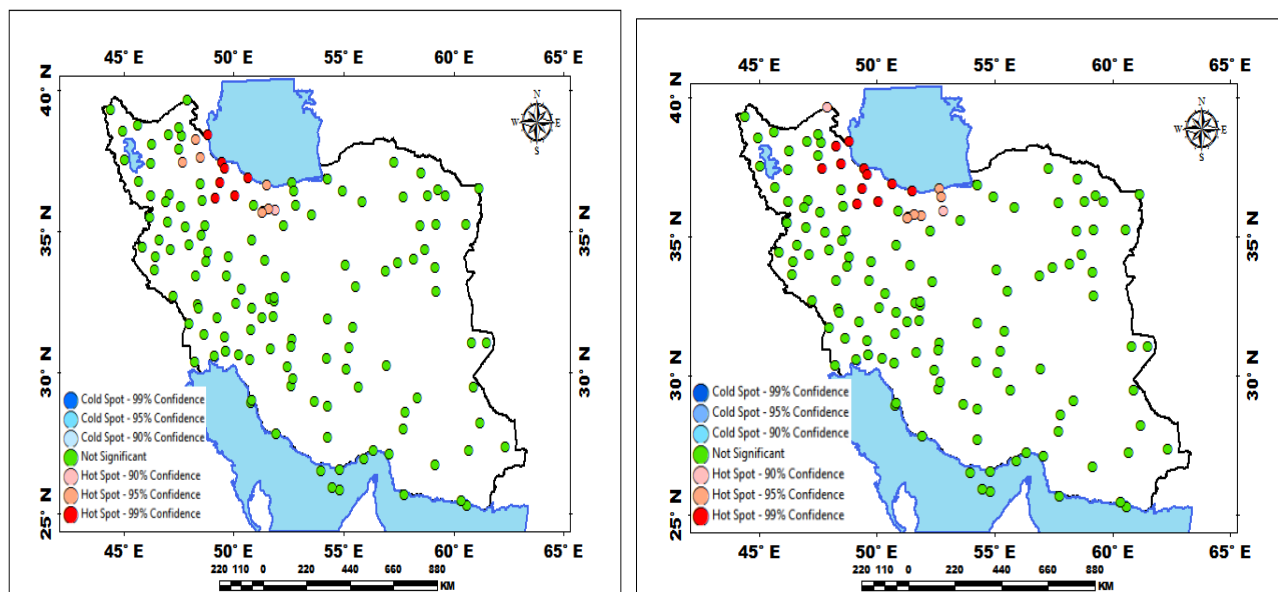
(12) High/low clustering of December.

(11) High/low clustering of November.

Figure 11: High/low clustering of monthly precipitation of (1) January to (12) December.



(1) Hot spot analysis of spring precipitation. (2) Hot spot analysis of winter precipitation.



(3) Hot spot analysis of autumn precipitation. (4) Hot spot analysis of summer precipitation.

Figure 12: Hot spot analysis (Getis-Ord Gi) of seasonal precipitation of (1) spring to (4) summer.

Spatial autocorrelation (Global Moran's I): The spatial autocorrelation (Global Moran's I) tool measures spatial autocorrelation based on both feature locations and feature values simultaneously. Given a set of features and an associated attribute, it evaluates whether the pattern expressed is clustered, dispersed, or random [36]. Global Moran's I characterizes only the average spatial pattern that is assumed to be equal across the whole study area and may not be suitable for assessing spatial autocorrelations of all stations [36]. The tool calculates the Moran's I Index value and both z-score and p-value to evaluate the significance of that index. The Spatial Autocorrelation tool returns five values: the Moran's I Index, Expected Index, Variance, z score, and p-value. Therefore, Global Moran's I test (value I) was employed, which examines whether the spatial distribution is dispersed ($I < 0$), random ($I \approx 0$), or clustered ($I > 0$) [75,76].

The Spatial Autocorrelation (Global Moran's I) tool is an inferential statistic, which means that the results of the analysis are always interpreted within the context of its null hypothesis. For the Global Moran's I statistic, the null hypothesis states that the attribute being analyzed is randomly distributed among the features in the study area; said another way, the spatial processes promoting the observed pattern of values is random chance. The p-value is not statistically significant. You cannot reject the null hypothesis. It is quite possible that the spatial distribution of feature values is the result of random spatial processes. The observed spatial pattern of feature values could very well be one of many, many possible versions of complete spatial randomness. The p-value is statistically significant, and the z-score is positive. You may reject the null hypothesis [36,46]. The seasonal precipitation was examined by Global Moran's I (Figure 10).

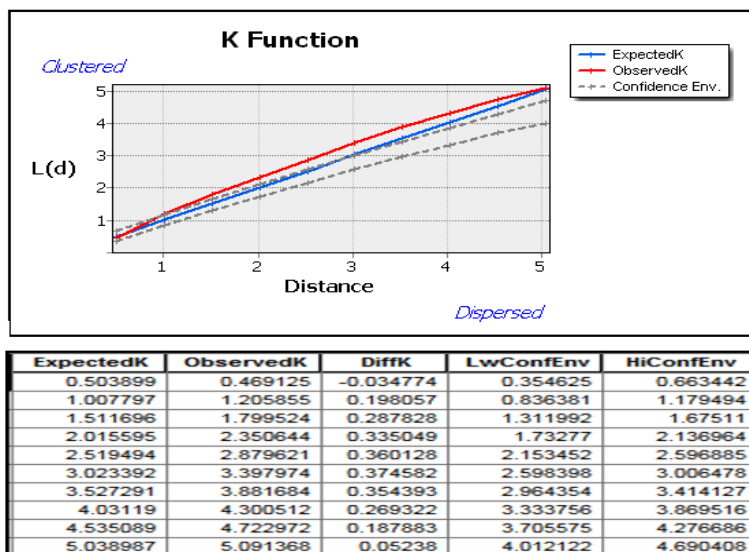
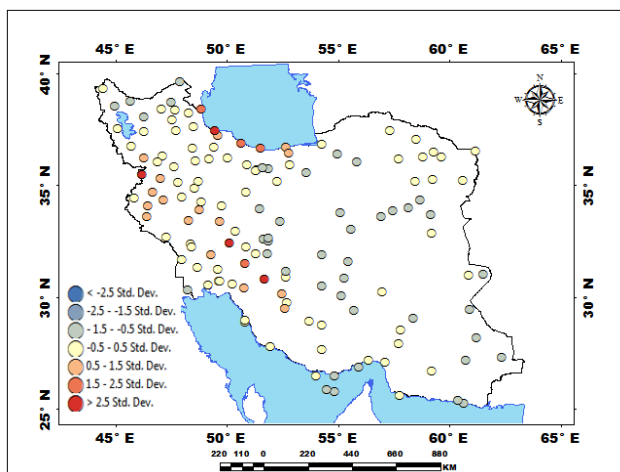
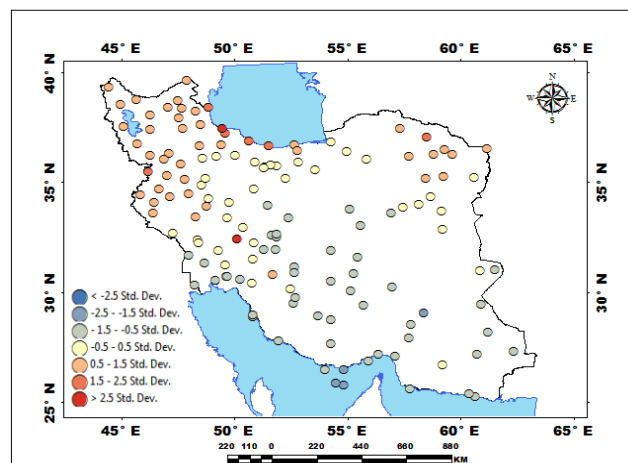


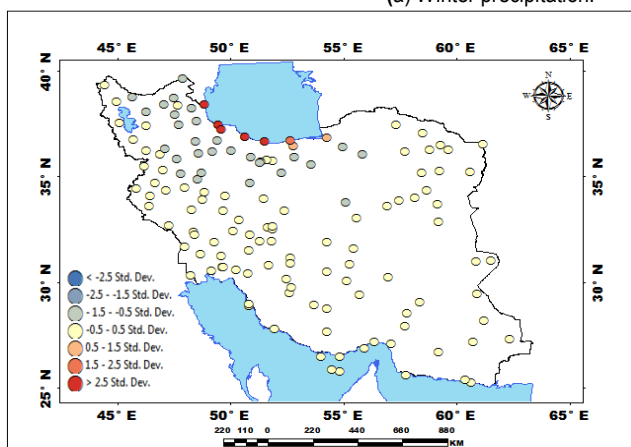
Figure 13: Multi-distance spatial cluster analysis of Iran precipitation.



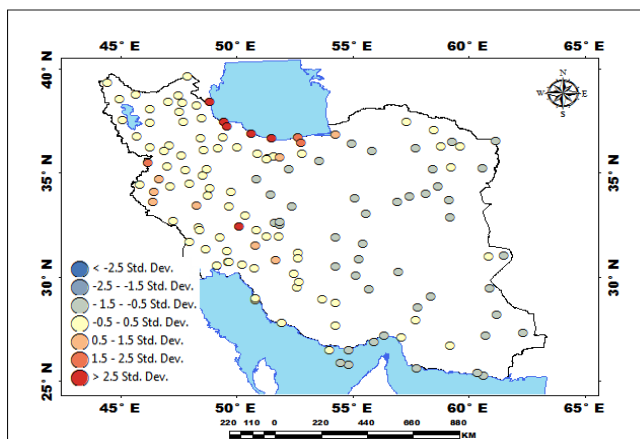
(a) Winter precipitation.



(b) Spring precipitation.



(c) Summer precipitation.



(d) Autumn precipitation.

Figure 14: The ordinary least squares analysis of seasonal precipitation of (1) winter to (4) autumn.

Exploratory regression and ordinary least squares: The exploratory regression tool evaluates all possible combinations of the input candidate explanatory variables, looking for OLS models that best explain the dependent variable within the context of user-specified criteria. The purpose of regionalization in this study is to provide predictions of monthly precipitation at stations. To achieve this purpose, Generalized Least Squares within subject framework is used to relate the precipitation characteristics of stations to the monthly rainfall data [77-81]. The seasonal precipitation was examined by ordinary least squares (Figure 14).

Results and Discussion

As pointed out, geostatistics and spatial statistics studies the variations of climatic variables or the elements which are not directly observable. These variations patterns are measured by several models. Concerning the effects of temporal-spatial factors on precipitation, two indicators that is, geostatistical models and spatial models, were found to influence precipitation. With respect to designing research algorithms, the model is done along with studying the geostatistical-spatial model. Studies have been conducted on the root mean square of measuring tool, on testing the research models, and on the effects of temporal-spatial factors on precipitation in Iran. The Geostatistical Analyst tool was used to study for spatial patterns in the state-wide distribution of monthly, seasonal and annual precipitation. Graphs were generated for each exploratory of precipitation spatial patterns described in section 4.1.1.

A normal distribution, the mean and mode will equal to the median, the skewness will equal one, and the Kurtosis will be equal to three. The histogram generated from the January data set had a mean of 3.6637 and a median of 3.5877, with a difference of 0.076, February data set had a mean of 3.498 and a median of 3.5025, with a difference of 0.0045, March data set had a mean of 3.7251 and a median of 3.7329, with a difference of 0.0078, April data set had a mean of 3.2296 and a median of 3.4688, with a difference of 0.2392, May data set had a mean of 18.686 and a median of 13.3, with a difference of 5.386, June data set had a mean of 6.596 and a median of 1.85, with a difference of 4.746, July data set had a mean of 4.492 and a median of 1.3, with a difference of 3.192, August data set had a mean of 5.3157 and a median of 0.8, with a difference of 4.516, September data set had a mean of 10.761 and a median of 1, with a difference of 9.761, November data set had a mean of 35.343 and a median of 27.15, with a difference of 8.193 and December data set had a mean of 47.157 and a median of 33.9, with a difference of 13.257. The January skewness value was 0.2392 and the Kurtosis was 2.5287, the February skewness value was 0.1045 and the Kurtosis was 3.3069, the March skewness value was 0.12778 and the Kurtosis was 3.1676, the April skewness value was -0.9311 and the Kurtosis was 3.8374, the May skewness value was 0.8476 and the Kurtosis was 2.6929, the June skewness value was 2.6041 and the Kurtosis was 9.598, the July skewness value was 3.2501 and the Kurtosis was 13.538, the August skewness value was 4.5468 and the Kurtosis was 34.738, the September skewness value was 27.679 and the Kurtosis was 4.9046, the November skewness value was 3.199 and the Kurtosis was 15.888 and the December skewness value was 3.2038, and the Kurtosis was 9.2538 (Figure 2). Also, a logarithmic transformation resulted in a mean of 5.5271, and a median of 5.5902. The skewness changed to -0.2623, and the kurtosis to 3.3697. The normality of monthly precipitation data was also used to assess data. The closer the data's quantile is to the straight line, the more normal the distribution will be. We used Voronoi diagrams to examine local variations of seasonal and annual precipitation series for every station. Voronoi diagrams are constructed from a series of polygons formed around the location of a sample point. The annually precipitation Voronoi maps displayed simple, mean, mode, cluster, entropy, median, standard deviation and interquartile range methods (Figure 4).

The seasonal precipitation Voronoi diagrams displayed standard deviation methods (Figure 5). Voronoi diagram displayed areas of high standard deviation relative to neighboring values. The map showed that the greatest differences in precipitation are concentrated in Western half of the map. The South Western quadrant of the Western half had especially high deviations. Trend analysis was used to study spatial patterns in the monthly precipitation. Two trends were discovered in the monthly precipitation. The red line projected against the XZ (North-South) plane represented a 2nd order trend. With a rotation angle of 110: the trend stretched from the N-NW to the S-SE. The blue line projected against the YZ plane at 45: is also a second order trend from NE to SW (Figure 6). We used Semivariogram/Covariance Cloud tool to estimate strength of statistical correlation as a function of distance and for all pairs of locations within a dataset and plots them as a function of the distance that separates the two locations.

This method modeling semivariograms and covariance functions fits a semivariograms or covariance curve to precipitation variations between annual, seasonal and monthly rainfall in Iran. The goal is to achieve the best fit (Figure 7). The results for Semivariogram/Covariance Cloud for winter precipitation are presented in Figures 7a and 7b. The red colored spots point out mainly distributed between ± 0.69 distances $h \times 10^{-1}$ from the North to South of Iran for the winter season and distributed between 0-2.11 distance $h \times 10^{-1}$ from the Western North to Eastern South of Iran for the spring season. The results for Semivariogram/Covariance Cloud for spring precipitation are presented in Figures 7c and 7d. The red colored spots point out mainly distributed between 0- 9.22 distances $h \times 10^{-1}$ from the North to South of Iran for the summer season. The results for Semivariogram/Covariance Cloud for summer precipitation are presented in Figures 7e and 7f. The red colored spots point out mainly distributed between 0-3.49 distances $h \times 10^{-1}$ from the Western North to Eastern South of Iran for the autumn season. The results for Semivariogram/Covariance Cloud for autumn precipitation are presented in Figures 7g and 7h. In this paper, we have studies the spatial variations patterns between annual, seasonal and monthly precipitation in Iran. The focus of the research presented herein was to geostatistical and spatially pattern on precipitation in Iran. All stations showed precipitation over Iran varies spatially at an annual, seasonal and monthly level with statistically significant results concentrated mostly in the North and Western parts of the country. A regionalization analysis in monthly precipitation was to estimate the temporal-spatial patterns variations in precipitation.

To accomplish this study, twenty-seven maps were created (Figures 8 and 9). The maps (Figure 8) were generated using all the default ArcGIS Geostatistical Analyst setting the Inverse Distance Weighting method for seasonal precipitation. Precipitation over Iran varies spatially and the winter precipitation range forecast using Inverse Distance Weighting for the whole country is 664.268 mm over the investigated period. The stronger spatial variations, the lower precipitation in general in Iran, while weaker spatial variations means larger precipitation in the country. The density of winter precipitation spatial distribution is in the South of Caspian Sea and some parts of the highlands in West to Eastern South of Iran the severe reduced distribution (Figure 8a). Precipitation spatial patterns over Iran varies and the spring precipitation range forecast using Inverse

Distance Weighting for the whole country is 195.98 mm over the investigated period that decreased from North and Western North to South and Eastern South in Iran. The density of spring precipitation spatial distribution is in the North and Western North (Figure 8b). On the summer scale, using inverse distance weighting, all of stations showed range about 380.183 mm that decreased from North to South in Iran. The density of summer precipitation spatial distribution is in the Caspian Sea (Figure 8c). The spatial distribution of precipitation in autumn using Inverse Distance Weighting showed the range about 688.73 mm that decreased toward center and south in Iran. The density of autumn precipitation spatial distribution is in the north of Iran (Caspian Sea) and some parts of the highlands (Figure 8d). In terms, spatial variations are very similar to the winter and autumn precipitation distribution. In our study, the highest percentage of precipitation variations spatially was observed in autumn and lowest in spring. Results showed for IDW method that all the RMSE indices calculated for seasonal periods indicate statistically significant for all seasons (autumn = 4.74, summer = 2.436, spring = 0.558 and winter = 1.68) especially of the spring season (errors mean is equal -0.0013).

Results of seasonal precipitation analysis using ArcGIS Geostatistical Analyst settings the Kriging and Cokriging are shown in Figure 9 for seasonal period. The spatial distribution of precipitation in autumn using Kriging showed the range of about 707.147 mm for Ordinary method, 648.109 mm for Simple method, 748.67 for Universal method, 673.97 for Disjunctive method, 787.892 for Empirical Bayesian method and 0.9 mm for Probability and Indicator methods that decreased toward Eastern South in Iran. Autumn precipitation in all stations showed severe variations spatially at a seasonal level with statistically significant results concentrated mostly in the Caspian Sea (Figure 9: 1-7). Results showed for Kriging method that all of the RMSE indices calculated for autumn periods indicate statistically significant for all methods (Simple = 4.56, Ordinary = 2.77, Empirical Bayesian = 165.81, Universal = 1.336, Indicator = 0.096, Probability=0.082 and Disjunctive = 82.51) especially of the Probability method (errors mean is equal to -0.0003). The spatial distribution of precipitation in spring using Kriging showed the range of about 390.47 mm for Ordinary method, 362.48 mm for Simple method, 148.81 for Universal method, 366.62 for Disjunctive method, 366.92 for Empirical Bayesian method and 0.9 mm for Probability and Indicator methods that decreased from North West toward South East in Iran. Spring precipitation at all stations showed severe variations spatially at a seasonal level with statistically significant results concentrated mostly in the North and Western North (Figure 9: 12-17). Results showed for Kriging method that all the RMSE indices calculated for spring periods indicate statistically significant for all methods (Simple = 24.7, Ordinary = 28,178, Empirical Bayesian = 23.63, Universal = 28.178, Indicator = 0.279, Probability = 0.292 and Disjunctive = 0.923) especially of the Indicator method (errors mean is equal to 0.017). The spatial distribution of precipitation in summer using Kriging showed the range of about 390.47 mm for Ordinary method, 362.48 mm for Simple method, 148.81 for Universal method, 366.62 for Disjunctive method, 366.92 for Empirical Bayesian method and 0.9 mm for Probability and Indicator methods that decreased toward South in Iran. Summer precipitation in all stations showed severe variations spatially at a seasonal level with statistically significant results concentrated mostly in the Caspian Sea (Figure 9: 8-11).

Results showed for Kriging method that all the RMSE indices calculated for summer periods indicate statistically significant for all methods (Simple = 39.126, Ordinary = 38.337, Empirical Bayesian = 34.412, Universal = 38.411, Indicator = 0.298, Probability = 0.304 and Disjunctive = 39.126) especially of the Indicator method (errors mean is equal 0.0056). The spatial distribution of precipitation in winter using Kriging showed the range of about 336.32 mm for Ordinary method, 279.9 mm for Simple method, 336.32 for Universal method, 280.24 for Disjunctive method, 620.98 for Empirical Bayesian method and 0.9 mm for Probability and Indicator methods that decreased the Western North toward Eastern South in Iran. Winter precipitation in all stations showed severe variations spatially at a seasonal level with statistically significant results concentrated mostly in the Western North (Figure 9: 18-24).

Results showed for Kriging method that all the RMSE indices calculated for winter periods indicate statistically significant for all methods (Simple = 73.898, Ordinary = 71.62, Empirical Bayesian = 69.51, Universal = 71.62, Indicator = 0.356, Probability = 0.35 and Disjunctive = 73898) especially of the probability method (errors mean is equal to 0.0028). We used global analysis method (i.e., global Moran's I indices) to estimate spatial patterns of distribution of stations by considering their locations. This method uses a measure known as the spatial autocorrelation coefficient to measure and test how observed locations are clustered/dispersed or random in space with respect to precipitation variations between annual, seasonal and monthly rainfall in Iran. The value of Moran's I statistic ranges from near + 1 indicating clustering of the data values to near -1 indicating dispersed pattern of the data values [43]. The positive values of Moran's I statistic with significant p-values and high Z-scores indicate spatially clustered data sets and negative Moran's I showed that the spatial pattern is more spatially dispersed [36].

The results for global Moran's I statistics for monthly precipitation are presented in Figure 10. All the Moran's I statistics estimated for months indicate statistically significant clustered spatial patterns with exception of February ($p < 0.02$). Figure 10 shows Moran's I statistics for all considered stations within all months. The High/Low Clustering (Getis-Ord General G) tool is an inferential statistic, which means that the results of the analysis are interpreted within the context of the null hypothesis. The null hypothesis for the High/Low Clustering (General G) statistic states that there is no spatial clustering of feature values. When the p-value returned by this tool is small and statistically significant, the null hypothesis can be rejected [36]. The results obtained for High/Low Clustering (Getis-Ord General G) statistics for any month are presented in Figure 11.

All the Getis-Ord General G statistics estimated for months indicate statistically significant High clusters spatial patterns for all months with exception of February and March (random) ($p < 0.02$). Hot Spot Analysis by estimating Getis-Ord Gi statistics identifies statistically significant spatial clusters of high values (hot spots) and low values (cold spots). The z-scores and p-values are measures of statistical significance that high z-score and small p-value for rainfall indicates a spatial clustering of high values. A low negative z-score and small p-value indicates a spatial clustering of low values. The higher (or lower) the z-score, the more intense the clustering. A z-score near zero indicates no apparent spatial clustering [30,36,57,81].

Figure 12 shows local Gi statistics and associated Gi Z scores for all considered stations' rainfall within seasonal period. The red colored spots (hot spots) point out clustering of high (positive) correlations that are mainly distributed in the North and Western North of Iran for the spring, summer and autumn and distributed in the West and Western South part of Iran for winter. The green colored insignificant spots without clustering are mainly distributed in the center and South and Eastern South of Iran for all seasons. There are not low Gi Z score values (cold spots)

with blue colored in Iran at seasonal level, during all seasons. Generally, positive scores in their spatial distribution are showing a WN-ES direction. This clustering of high Gi Z score over the Western North and Northern parts of Iran generally prevail and may be related to the precipitation amounts and seasonal precipitation temporal distribution (the Caspian Sea) since Eastern parts of Iran receive high precipitation than center and South ones. The Multi-Distance Spatial Cluster Analysis tool, based on Ripley's K-function, is another method to analyze the spatial pattern of rainfall. Ripley's K-function illustrates how the spatial clustering or dispersion of feature centroids changes when the neighborhood size changes [36,46]. When the observed K value is larger than the expected K value for a particular distance, the distribution is more clustered than a random distribution at that distance (scale of analysis). When the observed K value is smaller than the expected K value, the distribution is more dispersed than a random distribution at that distance.

Figure 13 show multi-distance spatial cluster analysis based on Ripley's K-function for all considered stations rainfall within annual period. The observed K value of annual precipitation for all stations is larger than the expected K value point out clustering that are mainly distributed in the North and Western North part of Iran. OLS method is applied to meteorological variables to make predictions. By using monthly and seasonal variables, precipitation prediction is made. Global Ordinary Least Squares (OLS) linear regression can be performed to generate predictions or to model a dependent variable in terms of its relationships to a set of explanatory variables [36].

The results for ordinary least squares for seasonal precipitation are presented in Figure 14. The regression residuals Figure 14 shows the under and over predictions from seasonal rainfall, and analyzing Figure 14 is an important step in finding a suitable model. Assessing model performance, both the Multiple R-Squared and Adjusted R-Squared values are measures of model performance. Figure 14 show results for Ordinary Least Squares for seasonal precipitation for all stations within all season are periods. The red colored areas point out that actual values are larger than the model estimated that are mainly distributed in the Western South part of Caspian Sea and West of Iran for winter and January, February, and March (Figure 14a) and for the spring season and April, May and June that are mainly distributed in the North, Western North, West and Eastern North of Iran (Figure 14b) and for the summer and July, August and September that are mainly distributed in the Western South of Caspian Sea of Iran (Figure 14c) and for autumn and October, November and December that are mainly distributed in the western south part of Caspian Sea and West part of Iran (Figure 14d). The blue colored areas point out actual values are smaller than the model estimated that are mainly distributed in the center and Eastern South of Iran for winter and January, February, and March (Figure 14a) and for spring and April, May and June that are mainly distributed in the center, Western South, East and Eastern South of Iran (Figure 14b) and for summer and July, August and September that are mainly distributed throughout Iran (an exception for Caspian Sea of Iran) (Figure 14c) and for autumn and months October, November and December that are mainly distributed in the center, South and East of Iran (Figure 14d). Testing was performed with determination coefficient (R^2) that R-Squared is a measure of goodness of fit. Its value varies from 0 to 1, with higher values being preferable.

Table 1 shows results for R-Squared for seasonal precipitation for all stations within all season are periods. Table 1 shows R-Squared for winter precipitation for all stations. R-Squared is 0.981 for winter, 0.938 for spring, 0.978 for summer and 0.988 for autumn. However, R-Squared values are suitable for goodness of fit for all seasons.

Conclusion

Using a Geostatistical-Spatial Statistics tool, especially one with a graphical - quantitative editor that allows the user to specify the model by drawing it on curtain -it is quite easy to add precipitation to a geostatistical - spatial model. A primary purpose of our study was zoning temporal-spatial patterns variations on precipitation. Our other aim was to examine the variations of various geostatistical - spatial patterns. In this study,

OID	Varname	Variable
0	Bandwidth	1.746
1	Residual squares	23821.578
2	Effective number	41.186
3	Sigma	15.526
4	AICc	1199.531
5	R2	0.980
6	R2 Adjusted	0.970
7	Dependent field	0
8	Explanatory field	1

(a) Winter.

OID	Varname	Variable
0	Bandwidth	1.859
1	Residual squares	18820.073
2	Effective number	37.797
3	Sigma	13.569
4	AICc	1157.821
5	R2	0.938
6	R2 Adjusted	0.915
7	Dependent field	0
8	Explanatory field	1

(b) Spring.

OID	Varname	Variable
0	Bandwidth	1.921
1	Residual squares	23239.474
2	Effective number	36.125
3	Sigma	14.957
4	AIcC	1183.231
5	R2	0.988
6	R2 Adjusted	0.984
7	Dependent field	0
8	Explanatory field	1

(c) Summer.

OID	Varname	Variable
0	Bandwidth	1.760
1	Residual squares	12010.644
2	Effective number	40.721
3	Sigma	10.999
4	AIcC	1102.430
5	R2	0.977
6	R2 Adjusted	0.968
7	Dependent field	0
8	Explanatory field	1

(d) Autumn.

Table 1: Geographically weighted regression and ordinary least squares of Iran seasonal rainfall.

six geostatistical, four regression and five spatial models were studied using monthly, seasonal and annual precipitation in Iran. 140 stations' precipitation was investigated using a geostatistical spatial model. Results indicated that there are various temporal-spatial variation patterns that affect precipitation in Iran. The findings also indicated that among the rainfall data which were influential on precipitation, seasonal then monthly and annual precipitation had the highest spatial variations on the rate of precipitation. The hypothesis for the geostatistical - spatial variations of the rainfall in Iran is also accepted. After all, the temporal-spatial patterns affects the precipitation rate in Iran and the geostatistical spatial model, can show the magnitude of these variations on the precipitation rate changes and can well examine the variation patterns.

Acknowledgement

This research was supported by Grant meeting of 19 in date of 2011.9.4 in Payame Noor University of Isfahan province. We also thank Payame Noor management and research committee of Payame Noor University.

References

- Benavides R, Montes F, Rubio A, Osoro K (2007) Geostatistical modelling of air temperature in a mountainous region of Northern Spain. *Agri Forest Meteorol* 146: 173-188.
- Fand BB, Tonnang HEZ, Kumar M, Bal SK, Singh NP et al. (2014) Predicting the impact of climate change on regional and seasonal abundance of the mealy bug *Phenacoccus solenopsis* Tinsley (Hemiptera: Pseudococcidae) using temperature-driven phenology model linked to GIS. *Ecol Modelling* 288: 62-78.
- Fares A, Awal R, Michaud J, Chu PS, Fares S et al. (2014) Rainfall-runoff modeling in a flashy tropical watershed using the distributed HL-RDHM model. *J Hydrol* 519: 3436-3447.
- Feizizadeh B, Shadman Roodposhti M, Jankowski P, Blaschke T (2014) A GIS-based extended fuzzy multi-criteria evaluation for landslide susceptibility mapping. *Computers Geosci* 73: 208-221.
- Keshavarzi B, Ebrahimi P, Moore F (2015) A GIS-based approach for detecting pollution sources and bioavailability of metals in coastal and marine sediments of Chabahar Bay, SE Iran. *Chemie der Erde – Geochemistry* 75: 185-195.
- Machiwal D, Jha MK (2014) Identifying sources of groundwater contamination in a hard-rock aquifer system using multivariate statistical analyses and GIS-based geostatistical modeling techniques. *J Hydrol: Regional Stud* (0).
- Martínez-Cob A (1996) Multivariate geostatistical analysis of evapotranspiration and precipitation in mountainous terrain. *J Hydrol* 174: 19-35.
- Masoud AA (2014) Groundwater quality assessment of the shallow aquifers west of the Nile Delta (Egypt) using multivariate statistical and geostatistical techniques. *J African Earth Sci* 95: 123-137.
- Ochoa-Rodriguez S, Wang LP, Gires A, Pina RD, Reinoso-Rondinel R (2014) Impact of spatial and temporal resolution of rainfall inputs on urban hydrodynamic modelling outputs: A multi-catchment investigation. *J Hydrol* (0).
- Olya HGT, Alipour H (2015) Risk assessment of precipitation and the tourism climate index. *Tourism Management* 50: 73-80.
- Siyal SH, Mörtberg U, Mentis D, Welsch M, Babelon I (2015) Wind energy assessment considering geographic and environmental restrictions in Sweden: A GIS-based approach. *Energy* 83: 447-461.
- Seyyedi H, Anagnostou EN, Beighley E, McCollum J (2015) Hydrologic evaluation of satellite and reanalysis precipitation datasets over a mid-latitude basin. *Atmospheric Res* 164-165: 37-48.
- Zhou W, Minnick MD, Mattson ED, Geza M, Murray KE (2015). GIS-based geospatial infrastructure of water resource assessment for supporting oil shale development in Piceance Basin of Northwestern Colorado. *Computers & Geosci* 77: 44-53.

14. Çelik R (2015) Temporal changes in the groundwater level in the upper Tigris Basin, Turkey, determined by a GIS technique. *J African Earth Sci* 107: 134-143.
15. Dummer TJB, Yu ZM, Nauta L, Murimboh JD, Parker L (2015) Geostatistical modelling of arsenic in drinking water wells and related toenail arsenic concentrations across Nova Scotia, Canada. *Sci Total Environ* 505: 1248-1258.
16. Elbeih SF (2015) An overview of integrated remote sensing and GIS for groundwater mapping in Egypt. *Ain Shams Eng J* 6: 1-15.
17. Haberlandt U (2007) Geostatistical interpolation of hourly precipitation from rain gauges and radar for a large-scale extreme rainfall event. *J Hydrol* 332: 144-157.
18. Huan J, Huang Y, Pontius Jr RG, Zhang Z (2015) Geographically weighted regression to measure spatial variations in correlations between water pollution versus land use in a coastal watershed. *Ocean & Coastal Management* 103: 14-24.
19. Javari M (2015) A study of impacts of temperature components on precipitation in Iran using SEM-PLS-GIS. *Earth Science & Climatic Change* 3: 1-14.
20. Karacan CÖ, Olea RA, Goodman G (2012) Geostatistical modeling of the gas emission zone and its in-place gas content for Pittsburgh-seam mines using sequential Gaussian simulation. *Int J Coal Geol* 90-91: 50-71.
21. Karagiannis-Voules DA, Odermatt P, Biedermann P, Khieu V, Schär F (2015) Geostatistical modelling of soil-transmitted helminth infection in Cambodia: Do socioeconomic factors improve predictions? *Acta Tropica*, 141, Part B(0): 204-212.
22. Mentis D, Hermann S, Howells M, Welsch M, Siyal SH (2015) Assessing the technical wind energy potential in Africa a GIS-based approach. *Renewable Energy* 83: 110-125.
23. Odeh IOA, Crawford M, McBratney AB (2006) Digital mapping of soil attributes for regional and catchment modelling, using ancillary covariates, statistical and geostatistical techniques. In A.B.M.P. Lagacherie & M. Voltz (eds.), *Developments in soil science*. Elsevier. pp. 31: 437-622
24. Pohlmann H (1993) Geostatistical modelling of environmental data. *CATENA* 20: 191-198.
25. Rivero RG, Grunwald S, Bruland GL (2007) Incorporation of spectral data into multivariate geostatistical models to map soil phosphorus variability in a Florida wetland. *Geoderma*, 140: 428-443.
26. Zewdu S, Suryabhagavan KV, Balakrishnan M (2014) Geo-spatial approach for soil salinity mapping in Sege Irrigation Farm, South Ethiopia. *J the Saudi Soc Agri Sci* (0).
27. Jha SK, Zhao H, Woldemeskel FM, Sivakumar B (2015) Network theory and spatial rainfall connections: An interpretation. *J Hydrol* 527: 13-19.
28. Plouffe CCF, Robertson C, Chandrapala L (2015) Comparing interpolation techniques for monthly rainfall mapping using multiple evaluation criteria and auxiliary data sources: A case study of Sri Lanka. *Environ Modelling & Software* 67: 57-71.
29. Agana N, Sefidmazgi MG, Homaifar A (2014) Analysis of extreme precipitation events. Paper presented at the Fourth International Workshop on Climate Informatics.
30. Luković J, Blagojević D, Kilibarda M, Bajat B (2015) Spatial pattern of North Atlantic oscillation impact on rainfall in Serbia. *Spatial Statistics* (0).
31. Santos M, Bateira C, Soares L, Hermenegildo C (2014) Hydro-geomorphologic GIS database in Northern Portugal, between 1865 and 2010: Temporal and spatial analysis. *Int J Disaster Risk Reduction* 10, Part A: 143-152.
32. Shi P, Wu M, Qu S, Jiang P, Qiao X (2015) Spatial distribution and temporal trends in precipitation concentration indices for the Southwest China. *Water Resources Management* 1-15.
33. Ahmadi S, Sedghamiz A (2008) Application and evaluation of kriging and cokriging methods on groundwater depth mapping. *Environmental Monitoring and Assessment* 138: 357-368.
34. Arslan H (2012) Spatial and temporal mapping of groundwater salinity using ordinary kriging and indicator kriging: The case of Bafra Plain, Turkey. *Agri Water Manage* 113: 57-63.
35. Babak O (2014) Inverse distance interpolation for facies modeling. *Stochastic Environ Res Risk Assessment* 28: 1373-1382.
36. ESRI (2014) *Spatial statistics tools*, ArcMap 10.3. ESRI, Redlands, California. ESRI, ArcMap 10.3. ESRI, Redlands, California.
37. Hengl T (2009) *A practical guide to geostatistical mapping*: Office for official publications of the European communities, Luxembourg.
38. Henley S (2012) *Nonparametric geostatistics*: Springer Science & Business Media.
39. Johnston K, Ver Hoef JM, Krivoruchko K, Lucas N (2001) *Using ArcGIS geostatistical analyst* (380): Esri Redlands.
40. Wu T, Li Y (2013) Spatial interpolation of temperature in the USA using residual kriging. *Applied Geography* 44: 112-120.
41. Aljani B, O'Brien J, Yarnal B (2008) Spatial analysis of precipitation intensity and concentration in Iran. *Theoretical and Applied Climatol* 94: 107-124.
42. Bone C, Wulder MA, White JC, Robertson C, Nelson TA (2013) A GIS-based risk rating of forest insect outbreaks using aerial overview surveys and the local Moran's I statistic. *Applied Geography* 40: 161-170.
43. Singh A, Damir B, Deep K, Ganju A (2015) Calibration of nearest neighbors model for avalanche forecasting. *Cold Regions Sci Technol* 109: 33-42.
44. <http://www.irimo.ir/englwd/720-Products-Services.html>
45. Christakos G (2012) *Modern spatiotemporal geostatistics*: Courier Corporation.
46. Hillman JIT, Gorman AR, Pecher IA (2015). Geostatistical analysis of seafloor depressions on the southeast margin of New Zealand's South Island - Investigating the impact of dynamic near seafloor processes on geomorphology. *Marine Geol* 360: 70-83.
47. Oliver M, Webster R (2014) A tutorial guide to geostatistics: Computing and modelling variograms and kriging. *CATENA* 113: 56-69.
48. Wang H, Chen Y, Pan Y, Li W (2015) Spatial and temporal variability of drought in the arid region of China and its relationships to teleconnection indices. *J Hydrol* 523: 283-296.
49. Keskin M, Dogru A, Balci F, Goksel C, Ulugtekin N (2015) Comparing spatial interpolation methods for mapping meteorological data in Turkey. In: A.N. Bilge, A.Ö. Toy & M.E. Günay (eds.), *Energy Systems and Management* (pp. 33-42): Springer International Publishing.
50. Wang X, Cui G, Wu F, Li C (2015) Analysis of temporal-spatial precipitation variations during the crop growth period in the Lancang River basin, South Western China. *Ecological Eng* 76: 47-56.

51. Cressie N (2015) Statistics for spatial data: John Wiley & Sons.
52. Akhtar MM, Zhonghua T, Sissou Z, Mohamadi B (2015) Assess arsenic distribution in groundwater applying GIS in capital of Punjab, Pakistan. Nat Hazards Earth Syst Sci Discuss 3: 2119-2147.
53. Pandey P, Kumar P, Tomar V, Rani M, Katiyar S (2015) Modelling spatial variation of fluoride pollutant using geospatial approach in the surrounding environment of an aluminium industries. Environ Earth Sci 1-12.
54. Hänsel S, Schucknecht A, Matschullat J (2015) The modified rainfall anomaly index (mRAI) - is this an alternative to the standardised precipitation index (SPI) in evaluating future extreme precipitation characteristics? Theoretical and Applied Climatol 1-18.
55. Hassen J (2014) A Geostatistical approach for mapping groundwater quality (Case study: Tehsil Sheikhpura). Int J Sci Res (IJSR) ISSN (Online), 2319-7064.
56. Magliano PN, Fernández RJ, Mercau JL, Jobbágy EG (2015) Precipitation event distribution in Central Argentina: spatial and temporal patterns. Ecohydrol 8: 94-104.
57. Ansari SM, Kale K (2014) Methods for crime analysis using GIS.
58. Ayuso JL, Ayuso-Ruiz P, García-Marín AP, Estévez J, Taguas EV (2015) Local analysis of the characteristics and frequency of extreme droughts in Málaga using the SPI (standardized precipitation index). In J.L. Ayuso Muñoz, J.L. Yagüe Blanco & S.F. Capuz-Rizo (eds.), Project Management and Engineering (pp. 167-179): Springer International Publishing.
59. Hjort J, Luoto M (2013) 2.6 Statistical methods for geomorphic distribution modeling. In J.F. Shroder (ed.), Treatise on Geomorphology (pp. 59-73). San Diego: Academic Press.
60. Sapriza-Azuri G, Jódar J, Navarro V, Slooten LJ, Carrera J (2015) Impacts of rainfall spatial variability on hydrogeological response. Water Resources Res 51: 1300-1314.
61. Zhang J, Han D, Freer J, Wagener T (2015) Analysis of spatial and temporal complexity of rainfall in the Brue catchment, UK. Paper presented at the EGU General Assembly Conference Abstracts.
62. Moustakas A (2015). Fire acting as an increasing spatial autocorrelation force: Implications for pattern formation and ecological facilitation. Ecological Complexity 21: 142-149.
63. Xu G, Cheng Y, Li P, Li Z, Zhang J (2015) Effects of natural rainfall on soil and nutrient erosion on sloping cropland in a small watershed of the Dan River, China. Quaternary Int (0).
64. Mennis J (2015) Asymmetric spatiotemporal interpolation. The Professional Geographer, 1-11.
65. Do VH, Thomas-Agnan C, Vanhems A (2015) Accuracy of areal interpolation methods for count data. arXiv preprint arXiv:1501.07506.
66. Ozelkan E, Bagis S, Ozelkan EC, Ustundag BB, Yucel M (2015) Spatial interpolation of climatic variables using land surface temperature and modified inverse distance weighting. Int J Remote Sensing 36: 1000-1025.
67. Verdin A, Rajagopalan B, Kleiber W, Funk C (2015) A bayesian kriging approach for blending satellite and ground precipitation observations. Water Resources Res 51: 908-921.
68. Bashir B, Fouli H (2015) Studying the spatial distribution of maximum monthly rainfall in selected regions of Saudi Arabia using geographic information systems. Arabian J Geosci 1-15.
69. Karagiannis-Voules DA, Biedermann P, Ekpo UF, Garba A, Langer E (2015) Spatial and temporal distribution of soil-transmitted helminth infection in sub-Saharan Africa: a systematic review and geostatistical meta-analysis. The Lancet Infectious Diseases, 15: 74-84.
70. Moore TW, Dixon RW (2015) A spatiotemporal analysis and description of hurricane Ivan's (2004) tornado clusters. Papers in Applied Geography 1: 192-196.
71. Bodnar L (2010) The use of ArcGIS Geostatistical analyst exploratory spatial data analysis.
72. Mahboubi P, Parkes M, Stephen C, Chan HM (2015) Using expert informed GIS to locate important marine social-ecological hotspots. J Environ Management (0).
73. Ahmad U, Ahmad SR, Luqman M (2015) A study of Polio disease in Pakistan using GIS approach.
74. Fuentes-Ramirez A, Mudrak E, Caragea P, Holzapfel C, Moloney K (2015) Assessing the impact of fire on the spatial distribution of *Larrea tridentata* in the Sonoran Desert, USA. Oecologia, 178: 473-484.
75. Réquia Jr WJ, Koutrakis P, Roig HL (2015) Spatial distribution of vehicle emission inventories in the Federal District, Brazil. Atmospheric Environ 112: 32-39.
76. Zhu XJ, Yu GR, Hu ZM, Wang QF, He HL (2015) Spatiotemporal variations of T/ET (the ratio of transpiration to evapotranspiration) in three forests of Eastern China. Ecological Indicators 52: 411-421.
77. Haddad K, Johnson F, Rahman A, Green J, Kuczera G (2015) Comparing three methods to form regions for design rainfall statistics: Two case studies in Australia. J Hydrol 527: 62-76.
78. Javari M (2010) Quantitative methods in climatology (Trend Models). Payam Resan Press, 30-70.
79. Sun W, Zhu Y, Huang S, Guo C (2015) Mapping the mean annual precipitation of China using local interpolation techniques. Theoretical and Applied Climatol 119: 171-180.
80. Sun Y, Bowman K, Genton M, Tokay A (2015) A Matérn model of the spatial covariance structure of point rain rates. Stochastic Environ Res and Risk Assessment, 29: 411-416.
81. Peeters A, Zude M, Käthner J, Ünlü M, Kanber R (2015) Getis-Ord's hot- and cold-spot statistics as a basis for multivariate spatial clustering of orchard tree data. Computers and Electronics in Agriculture 111: 140-150.